Article

Cell

Post-transcriptional Regulation of *De Novo* Lipogenesis by mTORC1-S6K1-SRPK2 Signaling

Graphical Abstract

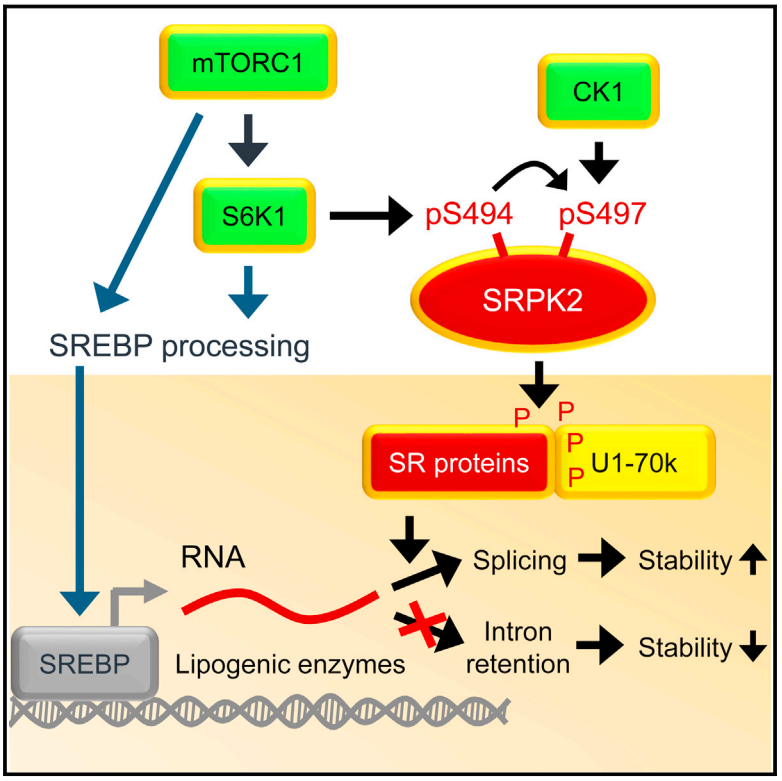

Highlights

- mTORC1-S6K1 and CK1 phosphorylate SRPK2 to induce its nuclear translocation
- SRPK2 activates SR proteins and U1-70K to promote splicing of lipogenic transcripts
- SRPK2 inhibition results in intron retention and mRNA instability of lipogenic genes
- Inhibition of SRPK2 signaling suppresses lipid metabolism and cancer cell growth

Authors

Gina Lee, Yuxiang Zheng, Sungyun Cho, ..., Joshua D. Rabinowitz, Lewis C. Cantley, John Blenis

Correspondence

job2064@med.cornell.edu

In Brief

An mTOR-dependent pathway is a key post-transcriptional regulator of lipogenic enzymes that are involved in tumor growth.

Lee et al., 2017, Cell *171*, 1545–1558
December 14, 2017
https://doi.org/10.1016/j.cell.2017.10.037

CellPress

Article

Cell

Post-transcriptional Regulation of *De Novo* Lipogenesis by mTORC1-S6K1-SRPK2 Signaling

Gina Lee,[1,2] Yuxiang Zheng,[1,3,10] Sungyun Cho,[1,10] Cholsoon Jang,[4] Christina England,[1] Jamie M. Dempsey,[5] Yonghao Yu,[6] Xiaolei Liu,[7] Long He,[1,2] Paola M. Cavaliere,[1] Andre Chavez,[1] Erik Zhang,[7] Meltem Isik,[8] Anthony Couvillon,[9] Noah E. Dephoure,[1] T. Keith Blackwell,[8] Jane J. Yu,[7] Joshua D. Rabinowitz,[4] Lewis C. Cantley,[1,3] and John Blenis[1,2,11,*]

[1]Meyer Cancer Center
[2]Department of Pharmacology
[3]Department of Medicine
Weill Cornell Medicine, New York, NY 10065, USA
[4]Lewis-Sigler Institute for Integrative Genomics and Department of Chemistry, Princeton University, Princeton, NJ 08544, USA
[5]Department of Cell Biology, Harvard Medical School, Boston, MA 02115, USA
[6]Department of Biochemistry, University of Texas Southwestern Medical Center, Dallas, TX 75390, USA
[7]Department of Internal Medicine, University of Cincinnati College of Medicine, Cincinnati, OH 45267, USA
[8]Joslin Diabetes Center and Department of Genetics, Harvard Medical School, Boston, MA 02215, USA
[9]Cell Signaling Technology, Danvers, MA 01923, USA
[10]These authors contributed equally
[11]Lead Contact
*Correspondence: job2064@med.cornell.edu
https://doi.org/10.1016/j.cell.2017.10.037

SUMMARY

mTORC1 is a signal integrator and master regulator of cellular anabolic processes linked to cell growth and survival. Here, we demonstrate that mTORC1 promotes lipid biogenesis via SRPK2, a key regulator of RNA-binding SR proteins. mTORC1-activated S6K1 phosphorylates SRPK2 at Ser494, which primes Ser497 phosphorylation by CK1. These phosphorylation events promote SRPK2 nuclear translocation and phosphorylation of SR proteins. Genome-wide transcriptome analysis reveals that lipid biosynthetic enzymes are among the downstream targets of mTORC1-SRPK2 signaling. Mechanistically, SRPK2 promotes SR protein binding to U1-70K to induce splicing of lipogenic pre-mRNAs. Inhibition of this signaling pathway leads to intron retention of lipogenic genes, which triggers nonsense-mediated mRNA decay. Genetic or pharmacological inhibition of SRPK2 blunts *de novo* lipid synthesis, thereby suppressing cell growth. These results thus reveal a novel role of mTORC1-SRPK2 signaling in post-transcriptional regulation of lipid metabolism and demonstrate that SRPK2 is a potential therapeutic target for mTORC1-driven metabolic disorders.

INTRODUCTION

A hallmark of living organisms is their ability to sense and couple various environmental cues to their growth. The mechanistic target of rapamycin complex 1 (mTORC1) integrates signals from growth factors, nutrients, and energy status, serving as a molecular rheostat, to regulate a wide range of anabolic and catabolic processes (Dibble and Manning, 2013; Gomes and Blenis, 2015; Saxton and Sabatini, 2017; Shimobayashi and Hall, 2014). mTORC1 is an atypical serine/threonine protein kinase that promotes cell growth through phosphorylation of multiple proteins including the ribosomal S6 kinase 1 (S6K1) and eIF4E-binding protein 1 (4E-BP1) (Ma and Blenis, 2009). Growth factors such as insulin activate PI3K-AKT signaling, thereby inhibiting the tumor suppressor tuberous sclerosis complex (TSC) 1/2, a negative regulator of mTORC1 (Manning and Toker, 2017; Shimobayashi and Hall, 2014). Loss-of-function mutations in *TSC1/2* lead to constitutive activation of mTORC1, which causes genetic tumor syndromes TSC and lymphangioleiomyomatosis (LAM) (Crino et al., 2006). Hyperactivation of mTORC1 by oncogenic PI3K-AKT and RAS-ERK pathways is also commonly observed in numerous cancers (Menon and Manning, 2008). Therefore, it is of great therapeutic importance to better understand how mTORC1 is able to control diverse cellular processes through regulation of newly discovered downstream targets.

Cancer cells regulate synthesis of macro-molecules to support sustained proliferation (DeBerardinis and Thompson, 2012; Vander Heiden et al., 2009). *De novo* lipid synthesis, for instance, provides fatty acids and cholesterol for expanding cell and organelle membranes (Gonzalez Herrera et al., 2015; Menendez and Lupu, 2007). This process begins with the production of acetyl coenzyme A (acetyl-CoA) from citrate or acetate by ATP citrate lyase (ACLY) or acyl-CoA synthetase short-chain (ACSS) family members, respectively. Fatty acid synthase (FASN) then catalyzes synthesis of fatty acids using acetyl-CoA and malonyl-CoA, which is produced from acetyl-CoA by acetyl-CoA carboxylase (ACC). The resulting palmitate is then utilized to generate a number of products, such as longer fatty acids via elongation, unsaturated fatty acids via stearoyl-CoA desaturase 1 (SCD1), phospholipids, and signaling lipids. For cholesterol biosynthesis,

hydroxymethylglutaryl-CoA synthase (HMGCS) catalyzes condensation of acetyl-CoA with acetoacetyl-CoA to generate HMG-CoA, which is converted to mevalonic acid by HMG-CoA reductase (HMGCR). This is then followed by multiple enzymatic reactions including those mediated by mevalonate diphosphate decarboxylase (MVD) and farnesyl diphosphate farnesyltransferase 1 (FDFT1). These key enzymes are often overexpressed in cancers (Currie et al., 2013; Menendez and Lupu, 2007). Thus, understanding the pertinent regulatory mechanisms holds promise for revealing potential therapeutic targets. One such regulator is the sterol regulatory element binding protein (SREBP) family of transcription factors, SREBP1 and 2. SREBPs are produced as inactive precursors bound to the endoplasmic reticulum membrane. Upon cellular lipid depletion, SREBPs are proteolytically processed to their active forms, translocate to the nucleus, and induce transcription of target genes (Horton et al., 2002). mTORC1 increases expression of lipogenic enzymes through SREBP activation, by both inactivating its negative regulators and increasing its expression level (Düvel et al., 2010; Li et al., 2010; Owen et al., 2012; Peterson et al., 2011; Han et al., 2015). However, little is known about the post-transcriptional regulation of lipogenic enzyme expression or whether the pro-lipogenic activity of mTORC1 extends to these events.

Cells employ a wide variety of post-transcriptional mechanisms for fine-tuning mRNAs and generating proteomic diversity, such as splicing, capping, polyadenylation, methylation, nuclear export, and stability (Fabian et al., 2010; Gilbert et al., 2016; Moore and Proudfoot, 2009; Park et al., 2005). These processes are regulated in part by various RNA-binding proteins, including serine/arginine-rich (SR) proteins and heterogeneous nuclear ribonucleoproteins (hnRNPs) (Chen and Manley, 2009). SR proteins are encoded by the *serine and arginine rich splicing factor* (*SRSF*) gene family and composed of RNA recognition motifs (RRM) and arginine/serine (RS)-repeat domains. They catalyze mRNA processing by directly binding to exons in pre-mRNA and recruiting proteins such as small nuclear ribonucleoproteins (SNRNPs) (Fu and Ares, 2014; Lee and Rio, 2015). The activity of SR proteins can be regulated via phosphorylation of the RS domain by SR protein kinases (SRPKs), which alters SR protein conformation, subcellular localization, and/or its interaction with other proteins (Ghosh and Adams, 2011).

Here, we reveal a previously unknown layer of mTORC1-dependent regulation of lipid metabolism that utilizes a new mTORC1-regulated effector kinase, SRPK2. Mechanistically, SRPK2 controls expression of lipogenic enzymes by inducing efficient splicing of their mRNAs rather than by affecting the synthesis of transcripts. Our findings uncover a mechanism by which nutrients and growth factors fine tune the regulation of splicing. Furthermore, our study highlights SRPK2 as a potential therapeutic target for mTORC1-driven diseases such as cancer and metabolic disorders.

RESULTS

Identification of SRPK2 as a Novel Downstream Target of mTORC1 Signaling

We previously performed a stable isotope labeling with amino acids in cell culture (SILAC)-based quantitative phospho-proteomics screen of mTORC1 signaling and identified SRPK2 as a putative downstream target (Figure 1A) (Yu et al., 2011). The putative phosphorylation sites in SRPK2, Ser494 and Ser497, are located in the linker region that splits the kinase domain and are evolutionarily conserved among vertebrates (Figure 1B). These phosphorylation sites were also detected in mTORC1 phospho-proteomics studies carried out by other groups (Hsu et al., 2011; Robitaille et al., 2013). To verify that mTORC1 regulates phosphorylation of SRPK2, we performed SDS-PAGE mobility shift assays. Upon insulin treatment to activate mTORC1 in HEK293E cells, the mobility of SRPK2 was dramatically decreased in a time-dependent manner, and the effect of insulin was completely blocked by rapamycin pre-treatment (Figure 1C), indicating the presence of insulin-regulated and rapamycin-sensitive phosphorylation(s). To further characterize Ser494 and Ser497 phosphorylation, we generated phospho-specific antibodies. Consistent with the gel mobility changes, insulin induced SRPK2 phosphorylation at Ser494 and Ser497, which was abolished by rapamycin treatment or SRPK2 knockdown (Figure 1D). We also tested SPRK2 phosphorylation in cell lines that display constitutively active mTORC1 activity. In these cells, SRPK2 was phosphorylated even in the absence of growth factors, which was blunted by mTORC1 inhibition with rapamycin (Figures 1E and 1F). Together, these results indicate that SRPK2 is phosphorylated at Ser494 and Ser497 in an mTORC1-dependent manner.

S6K1 Directly Phosphorylates SRPK2 at Ser494, which Primes for Ser497 Phosphorylation by CK1

We next sought to identify the kinase(s) that directly phosphorylates SRPK2. The Ser494 residue of SRPK2 is surrounded by a phosphorylation motif (RXRXX[S/T]) recognized by the basophilic protein kinase A, G, and C (AGC) kinase family (Pearce et al., 2010a) (Figure 2A). Since S6K1 is an AGC kinase directly activated by mTORC1, we examined whether S6K1 phosphorylates SRPK2 at Ser494. Efficient knockdown of S6K1 inhibited insulin-induced phosphorylation of SRPK2 at Ser494 (Figure 2B). In addition, the S6K1 inhibitor PF4708671 (Pearce et al., 2010b) reduced SRPK2 phosphorylation as robustly as rapamycin, Torin1 (mTOR active site inhibitor) (Thoreen et al., 2009), and MK2206 (AKT inhibitor) (Lindsley, 2010) (Figure 2C). Expression of an activated, rapamycin-resistant form of S6K1 (F5A-T389E-R3A) (Schalm and Blenis, 2002) induced SRPK2 phosphorylation even in the presence of rapamycin (Figure 2D). To further determine whether S6K1 directly phosphorylates SRPK2, we performed *in vitro* kinase assay. S6K1 immunoprecipitated from insulin treated cells, but not from rapamycin pre-treated cells, directly phosphorylated recombinant SRPK2 proteins (Figure 2E). Mutation of SRPK2-Ser494 to alanine (S494A) substantially abrogated SRPK2 phosphorylation by S6K1 (Figure 2E), demonstrating that Ser494 is the major S6K1 phosphorylation site in SRPK2. Collectively, these results indicate that S6K1 directly phosphorylates SRPK2 downstream of mTORC1 signaling.

Interestingly, we noted that Ser497 on SRPK2 is also phosphorylated in an mTORC1 and S6K1-dependent manner, and this phosphorylation is tightly correlated with phosphorylation of Ser494 (Figures 1 and 2). However, the phosphorylation motif surrounding Ser497 does not match the consensus AGC kinase

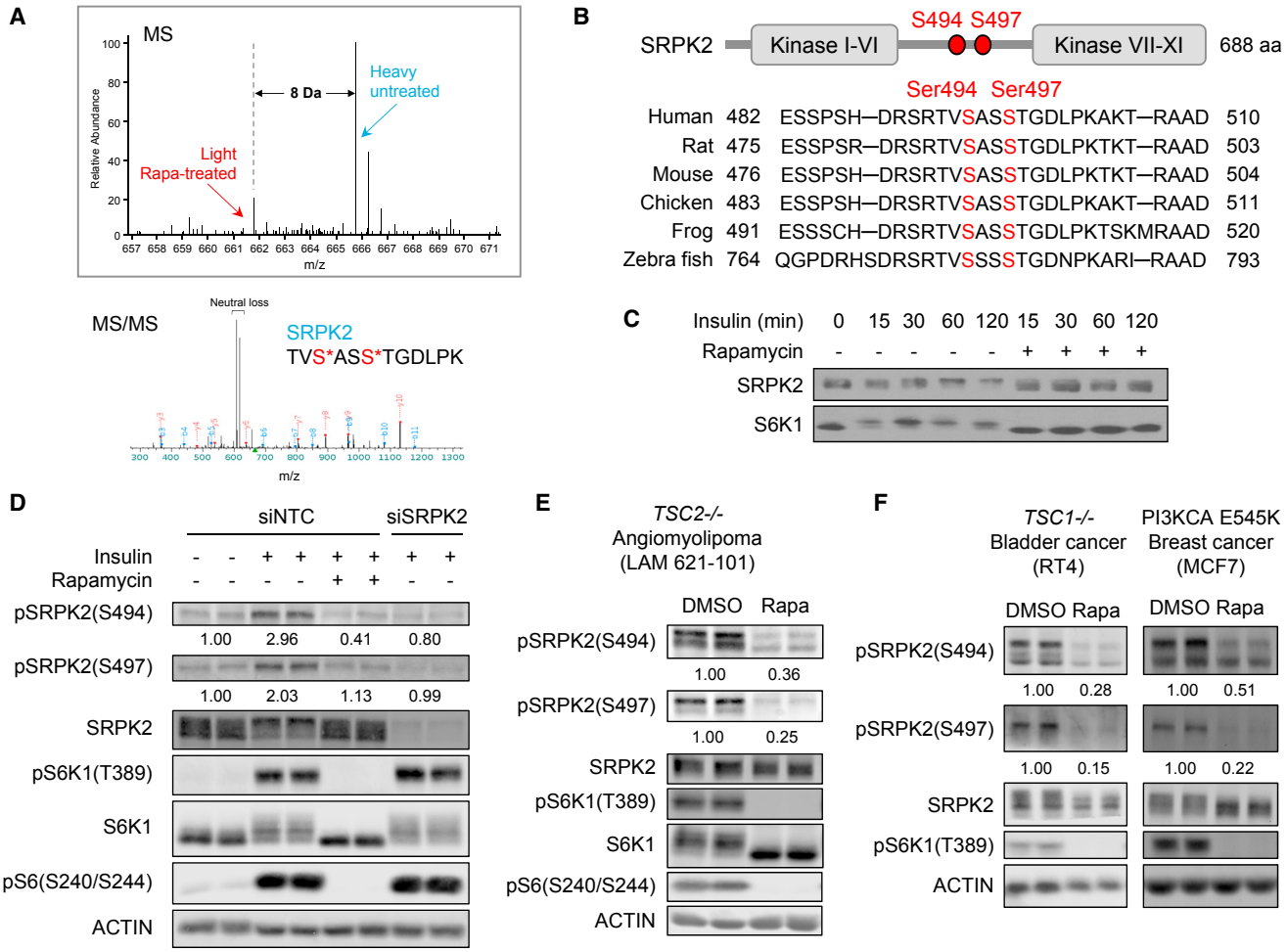

Figure 1. Identification of SRPK2 as a Downstream Target of mTORC1

(A) The SILAC-based phospho-proteomics analysis was performed on *Tsc2*$^{-/-}$ MEFs treated with vehicle or rapamycin (20 nM) for 2 hr. MS (top) and MS/MS (bottom) spectra of TVS*ASS*TGDLPK peptide from SRPK2 (asterisks indicate sites of phosphorylation) are shown.

(B) Schematics of SRPK2 protein domains (top) and amino acid conservation (bottom). The mTORC1-dependent phosphorylation sites are highlighted in red.

(C) Immunoblot analysis of HEK293E cells treated with insulin (100 nM) with or without rapamycin (Rapa, 20 nM) pre-treatment for 30 min after overnight serum starvation.

(D) Immunoblot analysis of HEK293E cells transfected with siRNAs targeting *SRPK2* or control. Cells were serum starved overnight and treated with insulin (100 nM) for 2 hr with or without rapamycin (20 nM) pre-treatment for 30 min.

(E and F) Immunoblot analysis of LAM 621-101 (E), RT4 (F, left), and MCF7 (F, right) cells treated with rapamycin (100 nM) for 24 hr with serum starvation. pSRPK2(S494) detects two bands in these cells.

substrate motif (Figure 2A). We therefore wanted to determine whether the phosphorylation at Ser494 primed Ser497 for phosphorylation. We knocked down endogenous *SRPK2* with a 3′ UTR-targeting short-hairpin RNA (shRNA), followed by expression of SRPK2 wild-type (SRPK2-WT) or non-phosphorylatable mutants (SRPK2-S494A or S497A) in *TSC2*-deficient cells (Figures 2F and 2G). Mutation of Ser494 to alanine dramatically inhibited phosphorylation of not only Ser494 but also Ser497, whereas mutation of Ser497 to alanine affected only its own phosphorylation (Figure 2G). These data indicate that Ser494 phosphorylation is crucial for Ser497 phosphorylation. Bioinformatics analysis revealed that Ser497 becomes a casein kinase 1 (CK1) target site when Ser494 is phosphorylated (pS/TXX[S/T]) (Figure 2H) (Flotow et al., 1990). Consistent with the primed substrate recognition mechanism, CK1 directly phosphorylated the recombinant SRPK2 proteins containing a phospho-mimetic mutation at Ser494 (S494D) (Figure 2I). This phosphorylation efficiency was decreased in the non-phosphorylated S494A mutant, and even more decreased in S494A/S497A mutant (Figure 2I), suggesting that Ser497 is the primary CK1 target residue. Taken together, these results demonstrate that CK1 functions as the SRPK2-Ser497 kinase following the priming phosphorylation of Ser494 by S6K1.

Phosphorylation of SRPK2 by mTORC1 Signaling Is Crucial for Its Nuclear Localization

SRPK2 was shown to translocate to the nucleus and phosphorylate downstream SR proteins (Jang et al., 2009; Zhou et al.,

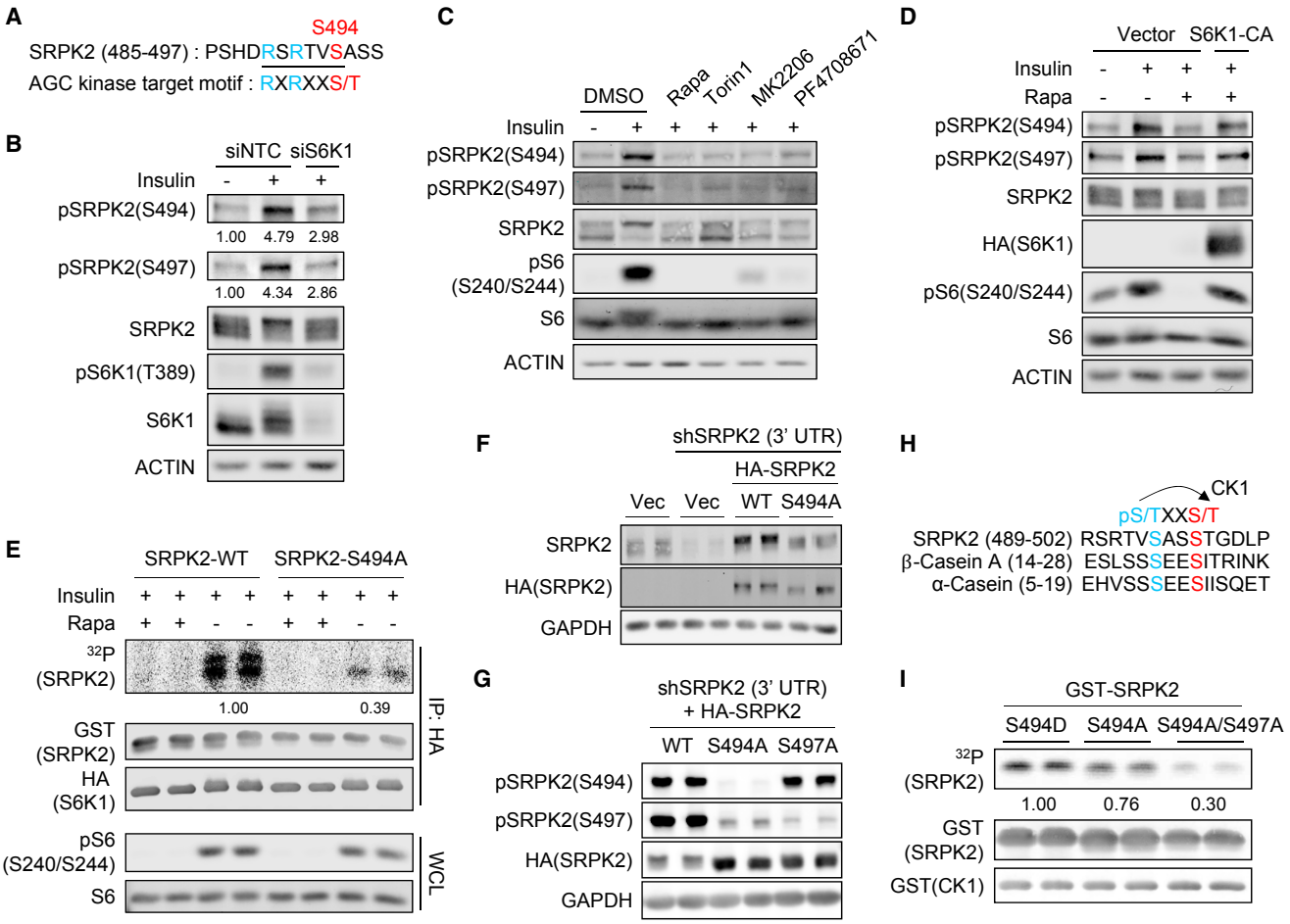

Figure 2. SRPK2 Phosphorylation at Ser494 by S6K1 Primes Ser497 Phosphorylation by CK1

(A) Alignment of SRPK2 amino acid sequence with AGC kinase phosphorylation motif.

(B) Immunoblot analysis of HEK293E cells transfected with siRNAs targeting *S6K1* or control. Cells were treated with insulin (100 nM) for 2 hr after overnight serum starvation.

(C) Immunoblot analysis of HEK293E cells. Cells were serum starved overnight and treated with the indicated small molecule inhibitors for 30 min, followed by insulin (100 nM) treatment for 2 hr. Rapamycin (100 nM), Torin1 (250 nM), MK2206 (10 μM), and PF4708671 (10 μM) were used.

(D) Immunoblot analysis of HEK293E cells transfected with HA-S6K1-CA (constitutively active S6K1) or vector. Cells were serum starved overnight and treated with insulin (100 nM) for 2 hr with or without rapamycin (20 nM) pre-treatment for 30 min.

(E) HEK293E cells transfected with HA-S6K1 were serum starved overnight and treated with insulin (100 nM) for 2 hr with or without rapamycin (20 nM) pre-treatment for 30 min. *In vitro* kinase assay was performed using HA-S6K1 immunoprecipitated (IP) from these cells. Recombinant GST-SRPK2-wild-type (WT) and S494A proteins were used as substrates. WCL, whole-cell lysates.

(F) Immunoblot analysis of LAM 621-101 cells expressing HA-SRPK2-WT or S494A. Endogenous *SRPK2* was knocked down with shSRPK2 targeting 3′ UTR.

(G) Immunoblot analysis of LAM 621-101 cells expressing HA-SRPK2-WT, S494A, or S497A. Endogenous *SRPK2* was knocked down with shSRPK2 targeting the 3′ UTR.

(H) Alignment of SRPK2 amino acid sequence with Casein sequences corresponding to the conserved CK1 substrate motif.

(I) *In vitro* CK1 kinase assay with recombinant GST-SRPK2-S494D, S494A, and S494A/S497A proteins as substrates.

2012). We therefore determined whether insulin and mTORC1 signaling regulates nuclear-cytoplasmic shuttling of SRPK2. Endogenous SRPK2 was predominantly localized in the cytoplasm in serum-starved HEK293E cells (Figure 3A). Insulin treatment induced nuclear accumulation of SRPK2, which was blocked by Torin1 pre-treatment (Figure 3A). Consistent with the nuclear accumulation of SRPK2, phosphorylation of SR proteins was increased by insulin (Figure 3B). Notably, in cell lines with high basal mTORC1 activity, SRPK2 predominantly localized to the nucleus (Figures 3C–3E). Inhibition of mTORC1 activity by rapamycin or Torin1 (Figures 3C and 3E) or by *TSC2* reconstitution (Figure 3D) induced cytoplasmic retention of SRPK2. These results show that insulin-mTORC1 signaling promotes nuclear localization of SRPK2.

We next investigated whether phosphorylation of SRPK2 at Ser494 and Ser497 is important for nuclear trafficking of SRPK2. In *TSC2*-deficient cells lacking endogenous *SRPK2* by knockdown (Figure 2F), exogenously expressed SRPK2-WT

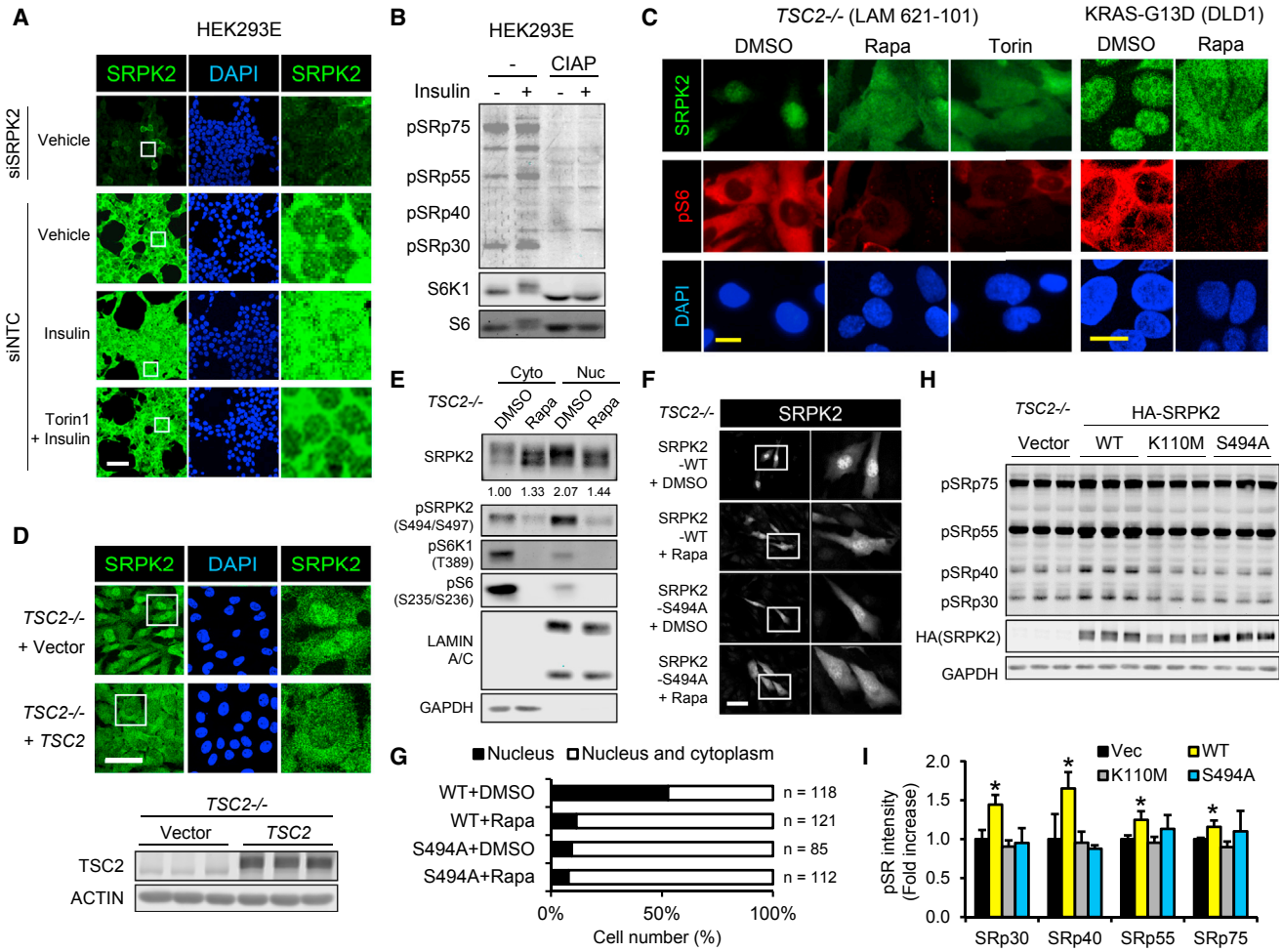

Figure 3. mTORC1-Dependent Phosphorylation of SRPK2 Induces Its Nuclear Translocation and SR Protein Phosphorylation

(A) Immunostaining of SRPK2 (green) in HEK293E cells transfected with siRNAs targeting *SRPK2* or control. Cells were serum starved overnight and treated with insulin (100 nM) for 2 hr with or without Torin1 (250 nM) pre-treatment for 30 min. Right panels show the enlarged images of the white boxes in the left panels. DAPI (blue), nucleus. Scale bar, 50 μm.

(B) Immunoblot analysis of HEK293E cells treated with insulin (100 nM) for 2 hr after overnight serum starvation. Half of the cell lysates were treated with calf intestinal alkaline phosphatase (CIAP) to dephosphorylate proteins.

(C) Immunostaining of SRPK2 (green) and pS6-S235/S236 (red) in the indicated cell lines treated with rapamycin (20 nM) or Torin1 (250 nM) for 2 hr. DAPI (blue), nucleus. Scale bars, 10 μm.

(D) Top, immunostaining of SRPK2 (green) in LAM 621-101 cells (*TSC2*$^{-/-}$) reconstituted with empty vector or *TSC2*. Right panels show the enlarged images of the white boxes in the left panels. DAPI (blue), nucleus. Scale bar, 50 μm. Bottom, immunoblot analysis of the reconstituted cells.

(E) Immunoblot analysis of cytoplasmic (Cyto) and nuclear fractions (Nuc) of LAM 621-101 cells treated with rapamycin (100 nM) for 4 hr after overnight serum starvation.

(F) Immunostaining of SRPK2 (white) in LAM 621-101 cells expressing SRPK2-WT or S494A. Endogenous *SRPK2* was knocked down with shSRPK2 targeting 3′ UTR. Cells were treated with vehicle or rapamycin (20 nM) for 2 hr. Right panels show the enlarged images of the white boxes in the left panels. Scale bar, 50 μm.

(G) Quantification of nuclear-cytoplasmic distribution of SRPK2 in (F). The number of cells counted is indicated.

(H) Immunoblot analysis of LAM 621-101 cells transfected with HA-SRPK2-WT, K110M (kinase dead), or S494A.

(I) Quantification of the average band intensity of phosphorylated SR proteins normalized to GAPDH in (H). n = 3. *p < 0.05. Data are represented as mean ± SD. See also Figure S1.

was localized in the nucleus (Figures 3F and 3G), whereas significantly less was observed to localize in the nucleus following rapamycin treatment (Figures 3F and 3G). In contrast, unlike SRPK2-WT, which accumulated in the nucleus of *TSC2*-deficient cells due to its constitutive phosphorylation, the non-phosphorylatable SRPK2-S494A, S497A, and S494A/S497A mutants were distributed to the cytoplasm and this localization was not further changed by rapamycin (Figures 3F, 3G, S1A, and S1B). Using *in silico* search, we found that SRPK2 contains a putative Importin alpha/beta-dependent nuclear-localization signal (NLS) near the Ser494 and Ser497 phosphorylation sites (Figure S1C) (Kosugi et al., 2009). Indeed, knockdown of *Importin-beta* prevented nuclear accumulation of SRPK2 (Figures S1D and S1E), suggesting that SRPK2 phosphorylation is important for Importin

alpha/beta-dependent NLS recognition and nuclear translocation (Nardozzi et al., 2010). Consistently, SRPK2-WT led to increased phosphorylation of SR proteins in *TSC2*-deficient cells (Figures 3H and 3I), whereas the kinase dead (K110M) or non-phosphorylatable (S494A) SRPK2 mutant had no effect (Figures 3H and 3I). Collectively, these results demonstrate that mTORC1-dependent SRPK2 phosphorylation induces SRPK2 nuclear localization and SR protein phosphorylation.

SRPK2 Regulates Expression of Lipid Biosynthetic Enzymes

SR proteins are implicated in many aspects of mRNA biogenesis such as transcription, splicing, export, translation, and stability (Chen and Manley, 2009; Fu and Ares, 2014). We therefore wanted to determine whether mTORC1-mediated regulation of SRPK2 alters RNA metabolism. To this end, we conducted whole-transcriptome microarray analyses of gene expression and exon/intron utilization on *TSC2*-deficient cells after rapamycin treatment or *SRPK2* knockdown (Figure S2A). Rapamycin affected mRNA levels of 842 genes (386 increased and 456 decreased) and splice isoforms of 3,590 genes. Knockdown of *SRPK2* changed mRNA levels of 471 genes (275 increased and 196 decreased) and splice isoforms of 3,809 genes (Figures 4A, S2B, and S2C). A fraction of genes (42 increased and 21 decreased) and splice isoforms (552 genes) were commonly changed by rapamycin treatment and *SRPK2* knockdown (Figure 4A).

Strikingly, among these 21 commonly decreased genes in both conditions, several encode enzymes crucial for lipid metabolism (highlighted in blue, Figure 4B) including those involved in *de novo* lipid synthesis such as *ACLY*, *ACSS2*, *HMGCS1*, *MVD*, and *FDFT1* (highlighted in red, Figure 4C). Real-time qPCR confirmed that the mRNA levels of these genes were significantly suppressed by mTORC1 inhibition using rapamycin or Torin1 treatment as well as by *SRPK2* knockdown (Figure 4D). Furthermore, expression of FASN and SCD1, key enzymes for fatty acid synthesis previously linked to mTORC1 signaling (Figure 4C) (Düvel et al., 2010; Peterson et al., 2011), was also substantially decreased by *SRPK2* knockdown (Figure S2D). Consistent with the decreased mRNA expression, protein levels of these enzymes were dramatically reduced by rapamycin as well as by *SRPK2* knockdown and knockout (Figures 4E and 4F). Overexpression of wild-type SRPK2, but not the non-phosphorylatable SRPK2 mutant, restored the expression of lipogenic enzymes in *SRPK2* knockdown cells (Figure 4G). Collectively, these results show that mTORC1-SRPK2 signaling regulates a broad gene expression program linked to lipid biosynthesis.

Lipogenic genes are transcriptionally regulated by SREBP1/2 transcription factors, which are regulated by mTORC1 (Horton et al., 2002; Caron et al., 2015). Thus, we determined whether SRPK2 induces lipid biosynthetic enzymes through SREBP1/2 in *TSC2*-deficient cells. In these cells, mTORC1 signaling is constitutively active independent of growth factors (Düvel et al., 2010; Zhang et al., 2014). Analysis of promoter regions covering 1 kb upstream of lipogenic genes (including SREBP-binding sites) showed that lipid deprivation by serum removal dramatically increased their promoter activity, which was suppressed by *SREBP1/2* knockdown (Figure 5A) (Horton et al., 2002). Surprisingly, despite remarkable reduction of mRNA and protein levels of lipogenic enzymes by *SRPK2* knockdown (Figure 4), we found no reduction in the promoter activity of these genes following *SRPK2* knockdown (Figure 5B). Indeed, *SCD1* and *ACSS2* displayed increased promoter activity, which may reflect a feedback loop (Figure 5B). In addition, the cleavage and nuclear translocation of SREBP1, which are key steps of SREBP1 activation (Horton et al., 2002), were induced by lipid deprivation but not affected by *SRPK2* deficiency (Figure 5C). Together, these results strongly suggest that SRPK2 controls expression of target genes by post-transcriptional mechanisms.

SRPK2 Increases mRNA Stability of Lipogenic Genes by Promoting Efficient Intron Splicing

We therefore investigated whether SRPK2 regulates expression of target genes via mRNA stability. We treated cells with actinomycin D to block transcription and measured the time-dependent turnover of lipogenic mRNAs (Tani and Akimitsu, 2012). The mRNA stability of *FDFT1*, *SCD1*, *ACLY*, *ACSS2*, *HMGCS1*, and *MVD* was markedly decreased by *SRPK2* knockdown as well as by rapamycin treatment (Figure 5D). However, rapamycin or *SRPK2* knockdown did not affect the mRNA stability of *phosphofructokinase, platelet* (*PFKP*) or *ribose 5-phosphate isomerase A* (*RPIA*) (Figure 5D), known mTORC1 transcriptional target genes in glycolysis and pentose phosphate pathway, respectively (Düvel et al., 2010). Importantly, the transcriptome array analysis showed that lipogenic genes including *ACSS2*, *FDFT1*, *HMGCS1*, and *MVD* retained introns upon rapamycin treatment or *SRPK2* knockdown (Figures S3A and S3B), indicating a reduced efficiency of intron splicing. In contrast, *PFKP* or *RPIA* did not exhibit consistent intron retention under these same conditions. Introns often contain stop codons, causing ribosome stalling and recruitment of the nonsense-mediated decay (NMD) machinery, and thereby triggering degradation of abnormal mRNAs (Chang et al., 2007; Isken and Maquat, 2008). The retained introns in these genes contained stop codons (Figure S3A), suggesting that NMD could contribute to the mRNA instability by *SRPK2* deficiency. To test this possibility, we inhibited NMD by knocking down a key NMD factor, *up-frameshift 1* (*UPF1*) (Chang et al., 2007), which restored the mRNA levels of lipogenic genes in *SRPK2* knockout cells to the levels in control cells (Figures 5E and S3C). Thus, NMD, at least in part, contributes to SRPK2-controlled regulation of mRNA stability.

Since SRPK2 downstream targets, the SR proteins, are RNA binding proteins, we determined whether SR proteins are involved in the regulation of lipogenic gene expression. Knockdown of some (*SRSF1/2/3*) but not all SR proteins resulted in a dramatic reduction in mRNA levels of lipogenic genes (Figures 5F and S3D), suggesting that a subset of SR proteins mediate the SRPK2-dependent regulation of lipogenic gene expression. *In silico* analysis predicted several SRSF1/2/3 binding sites in lipogenic genes (Table S1). Thus, we performed RNA-immunoprecipitation assay of SRSF1 and found that lipogenic transcripts bind to SRSF1 (Figures S3E and S3F). SR proteins do not contain enzymatic activities but rather participate in the recruitment of spliceosome complex proteins (e.g., small nuclear ribonucleoproteins) to induce splicing (Kohtz et al., 1994; Lee and Rio, 2015). To test whether mTORC1-SRPK2 signaling controls the interaction of SR proteins with spliceosomal proteins,

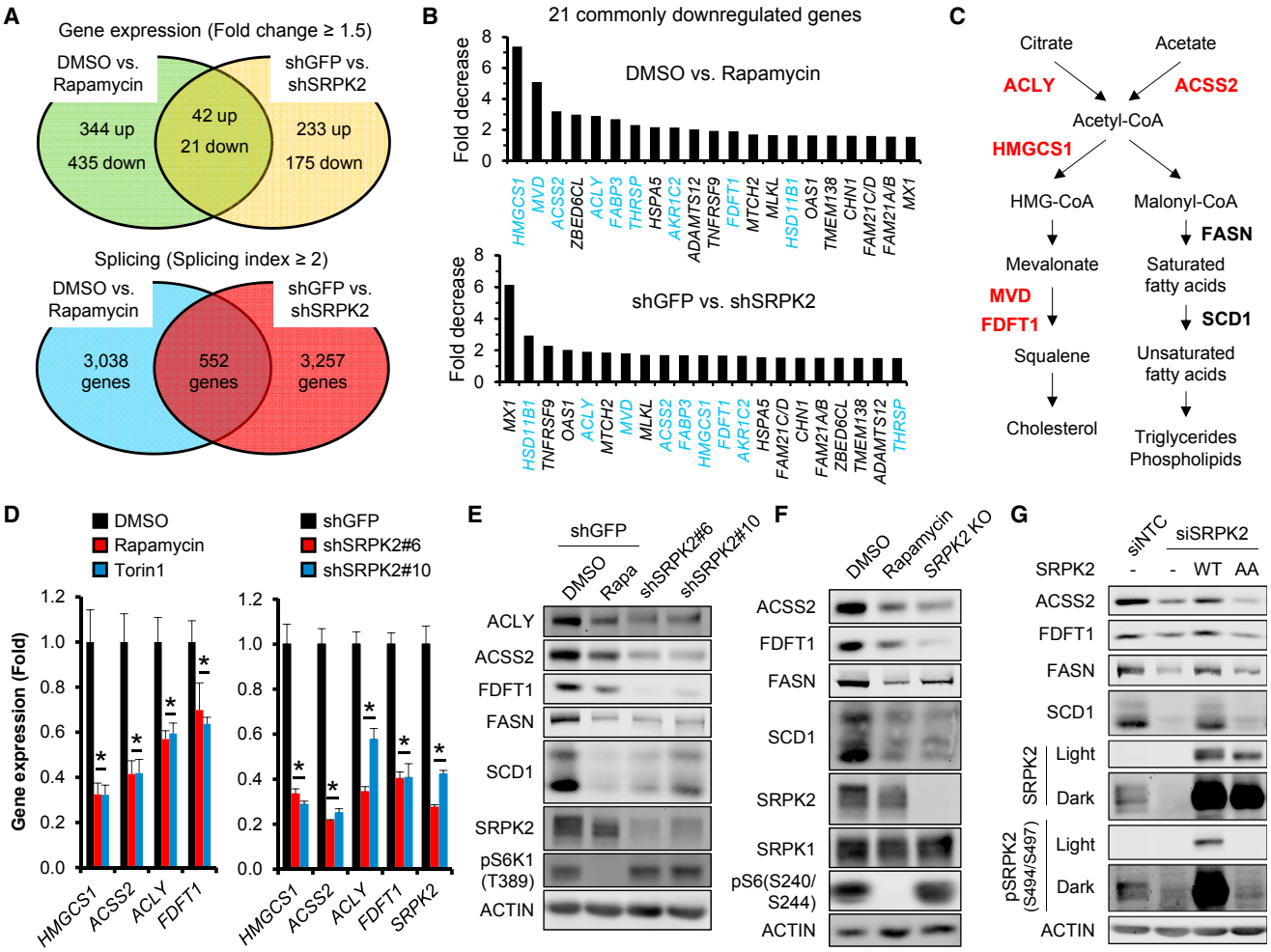

Figure 4. mTORC1 and SRPK2 Signaling Regulates Expression of Genes Involved in *De Novo* Lipid Synthesis

(A) Venn diagrams of the differentially regulated transcripts identified from the whole-transcriptome microarray analysis on LAM 621-101 cells. One analysis was conducted on the conditions where cells were treated with rapamycin (20 nM) or vehicle for 24 hr. The second analysis was conducted on the conditions where cells stably express shRNAs targeting *SRPK2* or *GFP*. Fold cutoff for the gene expression change (linear fold change) or splicing index (SI) is ≥1.5 or ≥2, respectively. SI = [Condition 1 (Probe intensity/Gene intensity)] / [Condition 2 (Probe intensity/Gene intensity]. n = 3. $p < 0.05$.

(B) Fold decreases of 21 commonly downregulated genes identified from the microarray analysis. Genes involved in lipid metabolism are highlighted in blue.

(C) Schematics of *de novo* lipogenesis. Genes identified from the microarray are highlighted in red.

(D) qPCR analysis of lipogenic genes in LAM 621-101 cells. Cells were treated with vehicle, rapamycin (20 nM), or Torin1 (250 nM) for 24 hr with serum starvation (left). Cells stably expressing shRNAs targeting *SRPK2* or *GFP* were serum starved overnight (right). n = 3. *$p < 0.05$. Data are represented as mean ± SD.

(E) Immunoblot analysis of LAM 621-101 cells stably expressing shRNAs targeting *SRPK2* or *GFP*. Cells were treated with rapamycin (20 nM) or vehicle for 24 hr with serum starvation.

(F) Immunoblot analysis of LAM 621-101 cells treated with rapamycin (100 nM) or vehicle for 24 hr with serum starvation. *SRPK2* KO, *SRPK2* CRISPR knockout cells.

(G) Immunoblot analysis of LAM 621-101 cells stably expressing mouse Srpk2-WT (wild-type) or AA (S488A/S491A, which corresponds to S494A/S497A in human SRPK2). Cells were transfected with siRNAs targeting *SRPK2* or control and serum starved overnight.

See also Figure S2.

we performed a proteomics-based interactome analysis for SRSF1 under vehicle- versus Torin1-treated conditions (Figure S4A). In Torin1-treated cells, we found reduced binding of SRSF1 with a small nuclear ribonucleoprotein U1 subunit 70 (SNRNP70/U1-70k) (Figure S4B; Table S2), a spliceosomal component required for splice site recognition and subsequent assembly of the spliceosome (Lee and Rio, 2015). Co-immunoprecipitation and immunoblotting confirmed that Torin1 significantly inhibited the binding of SRSF1 with U1-70k, which was accompanied with reduced SRSF1 phosphorylation (Figure 5G). Although not previously known to be regulated by the mTORC1 pathway, phosphorylation of SRSF1 by SRPK2 was shown to promote its interaction with U1-70k, thereby enhancing splicing of pre-mRNAs (Cho et al., 2011; Kohtz et al., 1994; Wang et al., 1998). Thus, our findings are consistent with these observations and further suggest a role for mTORC1 in regulating this

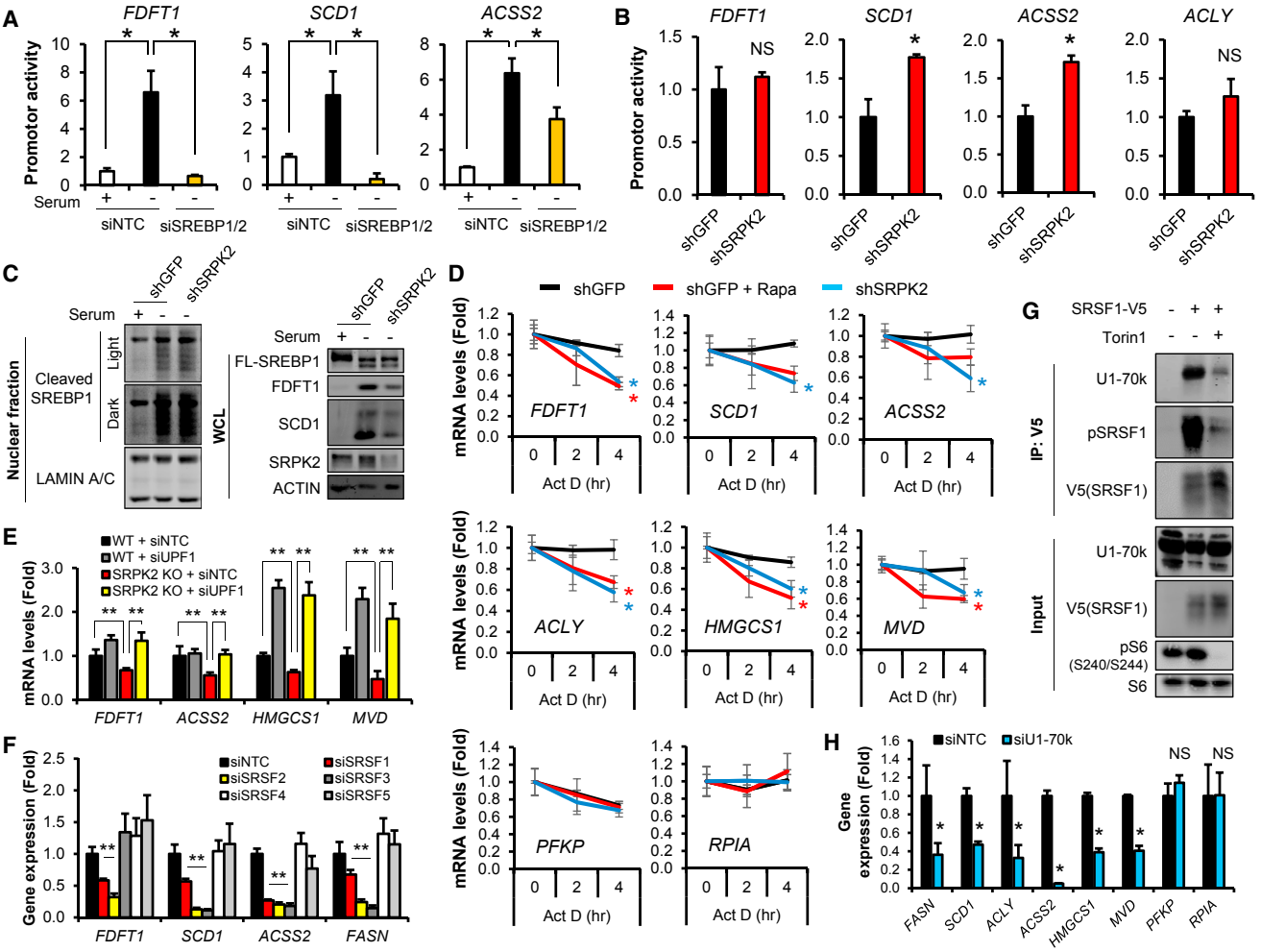

Figure 5. mTORC1 and SRPK2 Signaling Regulates mRNA Stability of Lipid Biosynthetic Genes

(A) Promoter activity analysis of LAM 621-101 cells transfected with promoter constructs with siRNAs targeting *SREBP1* and *SREBP2* (siSREBP1/2) or control in the presence or absence of serum. Promoter activity measured by renilla luciferase was normalized by cypridine luciferase. n = 2. Data are represented as mean ± SD.

(B) Promoter activity analysis of LAM 621-101 cells stably expressing shRNAs targeting *SRPK2* or *GFP* in the absence of serum. n = 2. Data are represented as mean ± SD.

(C) Immunoblot analysis of nuclear fractions or whole-cell lysates (WCL) in LAM 621-101 cells in the presence or absence of serum. FL-SREBP1, full-length SREBP1.

(D) Measurement of mRNA stability in LAM 621-101 cells stably expressing shRNAs targeting *SRPK2* or *GFP*. Cells were serum starved for 24 hr with rapamycin (100 nM) or vehicle treatment, followed by actinomycin D (Act D, 5 μg/mL) treatment for the indicated time points. qPCR was performed to measure mRNA levels of the indicated genes. n = 3. Data are represented as mean ± SD.

(E) qPCR analysis of WT or *SRPK2* knockout (KO) LAM 621-101 cells transfected with siRNAs targeting *UPF1* or control. n = 3. Data are represented as mean ± SD.

(F) qPCR analysis of LAM 621-101 cells transfected with siRNAs targeting each *SRSF* or control. n = 3. Data are represented as mean ± SD.

(G) Immunoblot analysis of HEK293E cells transfected with empty vector or SRSF1-V5. Cells were treated with Torin1 (250 nM) or vehicle for 4 hr. Immunoprecipitation (IP) was performed with anti-V5 antibody. 2% total cell lysate was loaded as an input.

(H) qPCR analysis of LAM 621-101 cells transfected with siRNAs targeting *U1-70k* or control. n = 3. Data are represented as mean ± SD.

*p < 0.05 and **p < 0.01. NS, not significant. See also Figures S3 and S4 and Tables S1 and S2.

interaction. Finally, knockdown of *U1-70k* increased intron retention and decreased expression of several lipogenic genes, but not *PFKP* or *RPIA* (Figures 5H and S3G). Together, these results suggest that mTORC1 signaling promotes the interaction of SR proteins with the spliceosomal protein U1-70k to induce efficient splicing of lipogenic pre-mRNAs.

SRPK2 Is Necessary for *De Novo* Synthesis of Cellular Fatty Acids and Cholesterol

We next examined whether the altered expression of lipid biosynthetic enzymes affects cellular lipid metabolism. To measure *de novo* lipid synthesis, we cultured *TSC2*-deficient cells in serum-free conditions with ^{14}C-labeled acetate and quantified

the amount of newly synthesized fatty acids and cholesterol by high-performance liquid chromatography (HPLC) (Figure 6A). Knockdown of *SREBP1/2*, as a positive control, decreased fatty acid and cholesterol synthesis (Figures S5A–S5C) (Düvel et al., 2010; Ricoult et al., 2016). Both stable and transient knockdown of *SRPK2* significantly reduced fatty acid and cholesterol synthesis (Figures 6A–6D) as did treatment with rapamycin or Torin1 (Figures 6E and 6F) (Düvel et al., 2010; Ricoult et al., 2016). We also measured *de novo* fatty acid synthesis in cells cultured with ^{13}C-glucose by liquid chromatography-mass spectrometry (LC-MS) (Kamphorst et al., 2013). This approach allows us to determine production of different fatty acid products. In serum-free conditions, we observed only a small effect on ^{13}C incorporation into the saturated fatty acids palmitate or stearate (Figures 6G and 6H). We did, however, observe a pronounced reduction in the synthesis of oleate, which is made from stearate by desaturation (Figures 6G and 6H). Under more physiological conditions, including the presence of serum, we observed a more substantial reduction in synthesis of both saturated and especially unsaturated fatty acids from glucose (Figures 6H–6J). Altogether, these results support the important role of mTORC1-SRPK2 signaling in regulating *de novo* lipid synthesis.

Inhibition of SRPK2 Blunts Cell Growth upon Lipid Starvation

Consistent with the reduced lipogenic potential, *SRPK2*-knocked down *TSC2*-deficient cells showed retarded cell proliferation (Figures 7A and 7B), which was more prominent when the growth was made more dependent on *de novo* lipid synthesis upon removal of lipids from the media (Figures 7A and 7B). Importantly, supplementation with lipoproteins (composed of cholesterol and fatty acids) or oleate (fatty acid) partially restored the growth of *SRPK2*-deficient cells (Figures 7C and 7D), indicating that the growth defect by *SRPK2* knockdown is in part due to an insufficient supply of lipids. To further validate the roles of SRPK2 on lipogenesis and cell growth, we employed an SRPK1/2 inhibitor, SRPIN340 (Fukuhara et al., 2006). SRPIN340 treatment reduced expression of lipogenic enzymes in a dose-dependent manner (Figures S6A–S6D). This inhibitory effect of SRPIN340 is likely due to SRPK2 suppression because SRPIN340 did not further reduce lipogenic gene expression in *SRPK2* knockout cells (Figure 7E). In addition, knockdown of *SRPK1*, a paralog of *SRPK2* (Wang et al., 1998), alone did not significantly affect lipogenic enzyme levels except SCD1 (Figure 7F). SRPIN340 treatment also dramatically suppressed *de novo* synthesis of fatty acids (Figure S6E) and cell growth in tumor cell lines with high mTORC1 activity (Figures 7G and S6F). To test the *in vivo* relevance of these findings in the context of cancer, we conducted xenograft growth studies with cell lines with high mTORC1 activity. Strikingly, both genetic (knockdown or knockout) and pharmacological inhibition of SRPK2 inhibited tumor growth across each of these multiple cancer cell line xenograft models (Figures 7H–7K, S6G, and S6H). Thus, these results further demonstrate that SRPK2 is a crucial downstream mediator for mTORC1-dependent lipogenesis, a process that contributes substantially to tumor growth.

DISCUSSION

Here, we report an unexpected link between the mTORC1 and SRPK2 signaling pathways. This signaling axis seems to be a key post-transcriptional regulator of lipid biosynthetic enzymes to support cell proliferation. Together with the known stimulatory function of mTORC1 on SREBP-dependent transcription, our study reveals that mTORC1 signaling utilizes both transcriptional and post-transcriptional mechanisms to amplify cellular lipid biogenesis (Figure S7).

Our findings indicate that the functional consequence of SRPK2 phosphorylation by mTORC1/S6K1 is its translocation from cytoplasm to nucleus (Figure 3). The downstream substrates of SRPKs, SR proteins, are involved in RNA metabolism and predominantly locate in the nucleus (Fu and Ares, 2014; Ghosh and Adams, 2011). Accordingly, SRPK2 nuclear localization is a critical node by which upstream signals (e.g., mTORC1/S6K1) regulate SRPK2 signaling. Previously, AKT was shown to induce SRPK2 phosphorylation at Thr492 to enhance its binding to 14-3-3 proteins (which often retain associated proteins in the cytoplasm) (Jang et al., 2009; Rittinger et al., 1999). However, AKT activation paradoxically resulted in SRPK2 nuclear accumulation (Jang et al., 2009). Since AKT activates mTORC1/S6K1 signaling, SRPK2 nuclear localization downstream of AKT is consistent with our results (Figure 3). It is possible that AKT temporally retains SRPK2 in the cytoplasm via 14-3-3 proteins, but S6K1 activation downstream of AKT subsequently induces SRPK2 nuclear translocation not only via SRPK2 phosphorylation, but possibly also via AKT inhibition through the well-established negative feedback mechanisms regulated by mTORC1 and S6K1 (Mendoza et al., 2011).

Another interesting aspect of SRPK2 phosphorylation is that the Ser494 phosphorylation by mTORC1/S6K1 induces subsequent Ser497 phosphorylation by CK1 (Figure 2). Although CK1 is constitutively active, its action on substrates is usually contingent upon priming phosphorylation by a different kinase (Flotow et al., 1990; Cheong and Virshup, 2011). For example, phosphorylation of DEPTOR on Ser293 and Ser299 by mTORC1 is followed by CK1, which creates a binding site on DEPTOR for βTrCP ubiquitin ligase (Duan et al., 2011; Gao et al., 2011). The amino acids around the SRPK2 phosphorylation sites are an Importin-alpha/beta-dependent NLS sequence (Figure S1C) (Kosugi et al., 2009), whose interaction with substrates is known to be enhanced by substrate phosphorylation around the NLS (Nardozzi et al., 2010). Thus, sequential phosphorylation by mTORC1/S6K1 and CK1 promotes efficient nuclear accumulation of SRPK2 and downstream signaling. It will be of great interest to investigate the kinetics of SRPK2 nuclear localization and how this results in additional nuclear phosphorylation events and mTORC1-dependent interaction with other proteins.

To support increased proliferation rates, cancer cells rewire their metabolism to meet the high demand for biosynthesis of macromolecules. Targeting metabolism has recently emerged as a new therapeutic strategy for cancer treatment (DeBerardinis and Thompson, 2012; Vander Heiden et al., 2009). Expression of enzymes for lipid biosynthesis such as *ACLY*, *ACC*, *FASN*, and *SCD1* is often elevated in tumors (Currie et al., 2013; Menendez

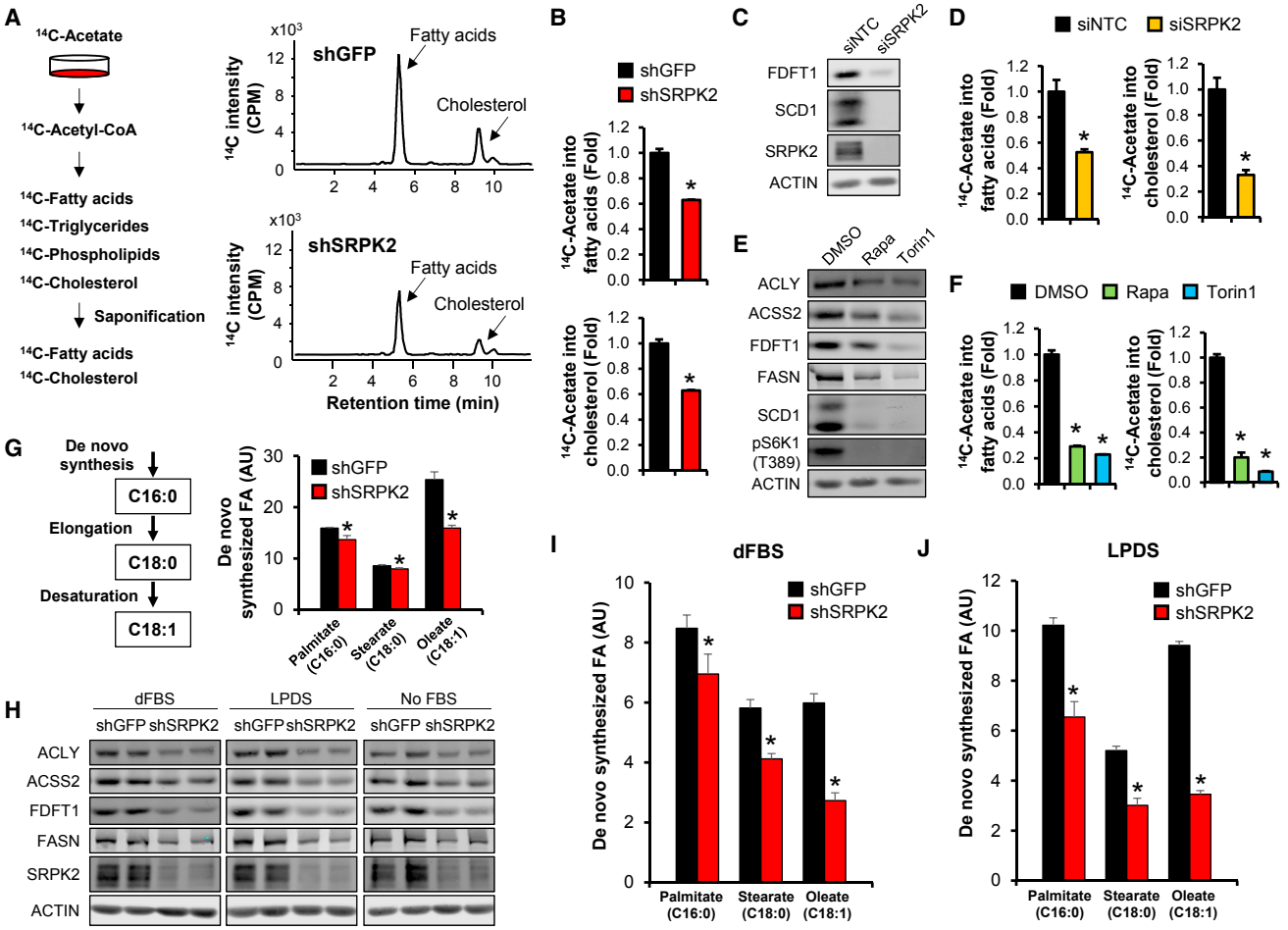

Figure 6. SRPK2 Is Necessary for *De Novo* Fatty Acid and Cholesterol Synthesis

(A) Left, schematic of radioactive ^{14}C-acetate incorporation assay for *de novo* fatty acid and cholesterol synthesis. Cells were cultured in serum-free medium. Right, HPLC analysis of radio-labeled fatty acids and cholesterol in LAM 621-101 cells stably expressing shRNAs targeting *SRPK2* or *GFP*.

(B) Quantification of integrated peak areas in (A) normalized to internal standard 13(S)-HODE. n = 2. Data are represented as mean ± SD.

(C and E) Immunoblot analysis of LAM 621-101 cells transfected with siRNAs targeting *SRPK2* or control (C). Cells were treated with rapamycin (20 nM) or Torin1 (250 nM) for 24 hr (E).

(D and F) Radioactive ^{14}C-acetate incorporation into fatty acids and cholesterol in LAM 621-101 cells transfected with siRNAs targeting *SRPK2* or control (D). Cells were treated with rapamycin (20 nM) or Torin1 (250 nM) for 24 hr (F). Graphs represent quantification of integrated HPLC peak areas normalized to internal standard 13(S)-HODE. n = 2. Data are represented as mean ± SD.

(G) LC-MS analysis of *de novo* fatty acid synthesis from U-^{13}C-glucose. LAM 621-101 cells stably expressing shRNAs targeting *SRPK2* or *GFP* were serum starved for 48 hr. Left, schematics of *de novo* fatty acid synthesis. Right, graph represents *de novo* synthesized fatty acids (FA). n = 4. Arbitrary unit (AU). Data are represented as mean ± SD.

(H) Immunoblot analysis of LAM 621-101 cells stably expressing shRNAs targeting *SRPK2* or *GFP*. Cells were grown without or with 10% dialyzed fetal bovine serum (dFBS) or lipoprotein-deficient serum (LPDS) for 48 hr.

(I and J) LC-MS analysis of *de novo* fatty acid synthesis from U-^{13}C-glucose. LAM 621-101 cells stably expressing shRNAs targeting *SRPK2* or *GFP* were grown with 10% dFBS (I) or LPDS (J). Graphs represent *de novo* synthesized fatty acids. n = 4. Data are represented as mean ± SD.

*$p < 0.05$. See also Figure S5.

and Lupu, 2007). Indeed, inhibition of these enzymes has been reported in certain cases to selectively kill cancer cells and retard tumor growth in xenograft models (Currie et al., 2013; Menendez and Lupu, 2007). SRPK2 is overexpressed in several cancer types including lung, colon, and acute myeloid leukemia (Gout et al., 2012; Jang et al., 2008; Wang et al., 2016). SRPK2 is a kinase and, therefore, a promising druggable target (Cohen, 2002; Fukuhara et al., 2006; Zhang et al., 2009). It is thus plausible to develop compounds that specifically inhibit SRPK2 for clinical use. Our results showed that SRPK2 inhibition with lipid deprivation inhibits cancer cell proliferation (Figure 7). Therefore, combination therapies using specific SRPK2 inhibitors and lipid uptake blockers such as CD36 antibodies (Pascual et al., 2017; Selwan et al., 2016) would also be a promising regimen for treatment of cancers with high dependency on mTORC1 signaling and lipid metabolism.

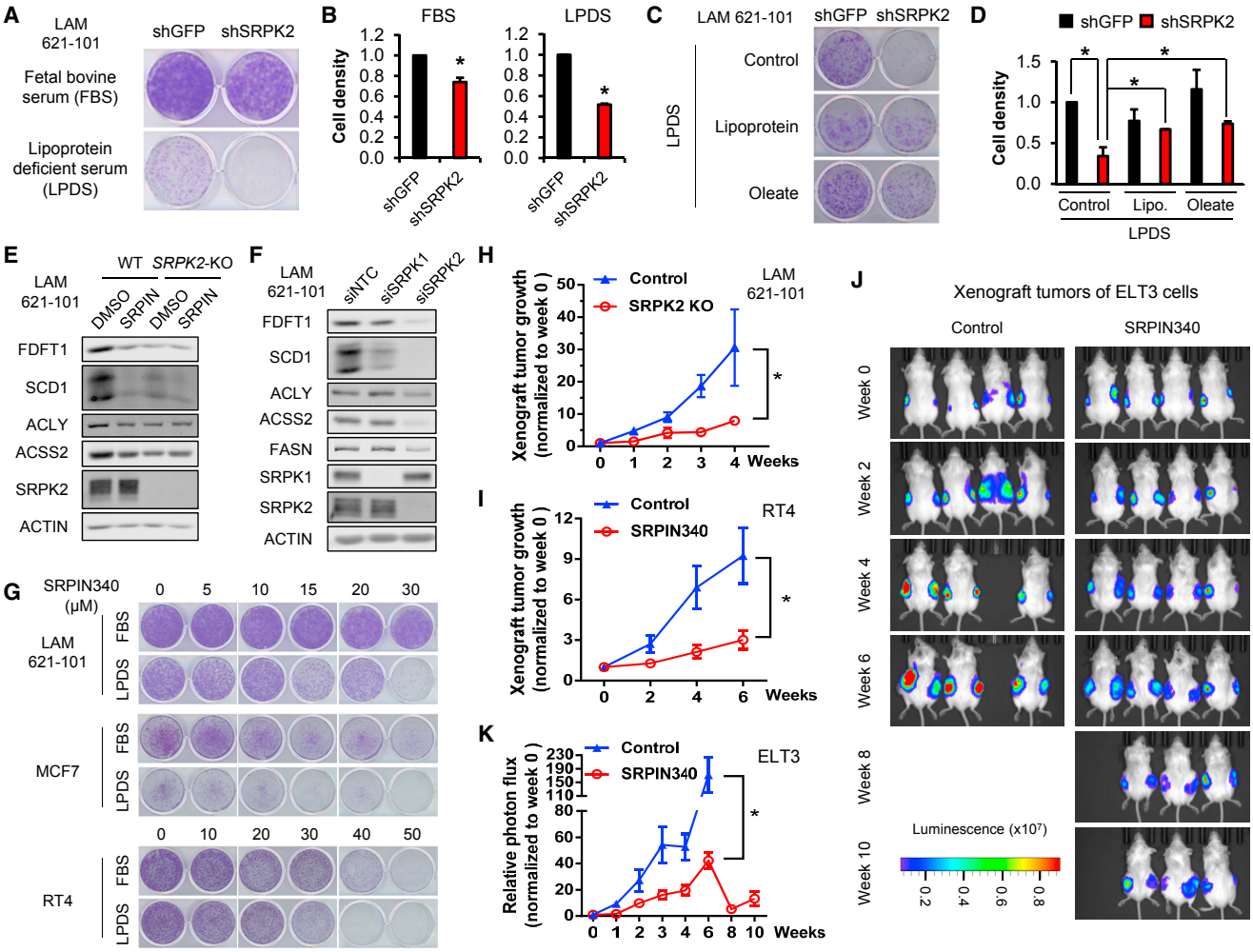

Figure 7. Inhibition of SRPK2 Blunts Cell Growth upon Lipid Starvation

(A) Crystal violet staining of LAM 621-101 cells stably expressing shRNAs targeting *SRPK2* or *GFP*.

(C) Crystal violet staining of LAM 621-101 cells stably expressing shRNAs targeting *SRPK2* or *GFP*. Lipoprotein (25 μg/ml), oleate-albumin (50 μM; oleate), or fatty acid-free albumin (25 μM; control) was supplemented to the media.

(B and D) Quantification of (A) and (C), respectively. Data are represented as mean ± SD.

(E) Immunoblot analysis of WT or *SRPK2* knockout (KO) LAM 621-101 cells treated with SRPIN340 (30 μM) for 48 hr with serum starvation.

(F) Immunoblot analysis of LAM 621-101 cells transfected with siRNAs targeting *SRPK1*, *SRPK2*, or control.

(G) Crystal violet staining of the indicated cell lines treated with SRPIN340 at the indicated concentrations.

(H) Xenograft tumor growth assays of WT (control) or *SRPK2* knockout (KO) LAM 621-101 cells. Graph represents the fold change of tumor size relative to week 0 (week 0 = tumor formation). n = 8 tumors. Data are represented as mean ± SEM.

(I–K) Xenograft tumor growth assays of RT4 (I) and ELT3 (*Tsc2*$^{-/-}$ rat leiomyoma)-luciferase cells (J and K) treated with SRPIN340. (I) Graph represents the fold change of tumor size relative to week 0. (J) Bioluminescent imaging of mice bearing ELT3-luciferase tumors. (K) Graph represents the fold change of total photon flux relative to week 0 in (J). n = 6–8 tumors. (I and K) Data are represented as mean ± SEM.

*p < 0.05. See also Figures S6 and S7.

STAR★METHODS

Detailed methods are provided in the online version of this paper and include the following:

- KEY RESOURCES TABLE
- CONTACT FOR REAGENT AND RESOURCE SHARING
- EXPERIMENTAL MODEL AND SUBJECT DETAILS
  - Cell lines
  - Mice
  - Microbe strains
- METHODS DETAILS
  - Antibodies and small molecule inhibitors
  - Gene expression analysis and measurement of mRNA stability
  - Human whole transcriptome microarray
  - HPLC analysis of *de novo* lipid synthesis
  - LC-MS analysis of saponified fatty acids

SUPPLEMENTAL INFORMATION

Supplemental Information includes seven figures and three tables and can be found with this article online at https://doi.org/10.1016/j.cell.2017.10.037.

AUTHOR CONTRIBUTIONS

G.L. and J.B. designed the study. G.L. conducted all the experiments unless otherwise indicated. Y.Z. performed the HPLC analysis of lipids. C.J. performed the LC-MS analysis of lipids and CRISPR/Cas9 knockout. S.C., C.E., J.M.D., L.H., and A. Chavez performed some of the cellular and molecular biological experiments. X.L. and E.Z. performed mouse experiments. P.M.C. performed proteomics-based interactome analysis. Y.Y. performed phospho-proteomics analysis. M.I. performed bioinformatics analysis. A. Couvillon provided the phospho-specific antibodies for SRPK2. G.L. and J.B. wrote the manuscript. All authors, including N.E.D., T.K.B., J.J.Y., J.D.R., and L.C.C., discussed the results and commented on the manuscript.

ACKNOWLEDGMENTS

We thank members of Blenis lab, Dennis Liang Fei, Jared Johnson, Florian Karreth, Jihye Yun, Xu Xu, and Ann-Hwee Lee (Weill Cornell Medicine) for discussions and technical assistance. We also would like to thank Brendan Manning (Harvard School of Public Health), Hong-Wen Tang and Norbert Perrimon (Harvard Medical School), Hanseul Yang (Rockefeller University), and Keqiang Ye (Emory University) for discussions. This work was supported by NIH grants R01 CA046595, R01 HL121266, and R01 GM051405 (to J.B.), P01 CA120964, R01 GM041890, and R35 CA197588 (to L.C.C.), R01 CA16359 (to J.D.R.), R01 HL098216 and R01 DK098331 (to J.J.Y.), R01 GM62891, R01 GM122610, and R01 AG54215 (to T.K.B.), and R01 GM114160 (to Y.Y.); Stand Up to Cancer grant SU2C-AACR-DT0509 (to J.D.R.); the Ellison Medical Foundation (to T.K.B.); and the Welch Foundation (I-1800; to Y.Y.). This work was partially supported by fellowships from the LAM Foundation (LAM00100F01-14), the Tuberous Sclerosis Alliance (TSA-01-14), and the National Research Foundation of Korea (2012R1A6A3-A03039825 to G.L.), the Department of Defense Breast Cancer Research Program (W81XWH-13-1-0251 to Y.Z.), the Kwanjeong Educational Foundation (to S.C.), the American Diabetes Association (1-17-PDF-076 to C.J.), and the American Federation for Aging Research (to M.I.). L.C.C. is a founder and member of the Board of Directors and Scientific Advisory Board of Agios Pharmaceuticals, a company developing drugs that target metabolism for cancer therapy; he is also a founder and member of the Scientific Advisory Board of Petra Pharmaceuticals and receives research support from Petra.

Received: August 29, 2017
Revised: October 3, 2017
Accepted: October 23, 2017
Published: November 16, 2017

REFERENCES

Boersema, P.J., Aye, T.T., van Veen, T.A.B., Heck, A.J.R., and Mohammed, S. (2008). Triplex protein quantification based on stable isotope labeling by peptide dimethylation applied to cell and tissue lysates. Proteomics *8*, 4624–4632.

Caron, A., Richard, D., and Laplante, M. (2015). The roles of mTOR complexes in lipid metabolism. Annu. Rev. Nutr. *35*, 321–348.

Chang, Y.-F., Imam, J.S., and Wilkinson, M.F. (2007). The nonsense-mediated decay RNA surveillance pathway. Annu. Rev. Biochem. *76*, 51–74.

Chen, M., and Manley, J.L. (2009). Mechanisms of alternative splicing regulation: Insights from molecular and genomics approaches. Nat. Rev. Mol. Cell Biol. *10*, 741–754.

Cheong, J.K., and Virshup, D.M. (2011). Casein kinase 1: Complexity in the family. Int. J. Biochem. Cell Biol. *43*, 465–469.

Cho, S., Hoang, A., Sinha, R., Zhong, X.-Y., Fu, X.-D., Krainer, A.R., and Ghosh, G. (2011). Interaction between the RNA binding domains of Ser-Arg splicing factor 1 and U1-70K snRNP protein determines early spliceosome assembly. Proc. Natl. Acad. Sci. USA *108*, 8233–8238.

Cohen, P. (2002). Protein kinases–the major drug targets of the twenty-first century? Nat. Rev. Drug Discov. *1*, 309–315.

Crino, P.B., Nathanson, K.L., and Henske, E.P. (2006). The tuberous sclerosis complex. N. Engl. J. Med. *355*, 1345–1356.

Csibi, A., Lee, G., Yoon, S.-O., Tong, H., Ilter, D., Elia, I., Fendt, S.-M., Roberts, T.M., and Blenis, J. (2014). The mTORC1/S6K1 pathway regulates glutamine metabolism through the eIF4B-dependent control of c-Myc translation. Curr. Biol. *24*, 2274–2280.

Currie, E., Schulze, A., Zechner, R., Walther, T.C., and Farese, R.V., Jr. (2013). Cellular fatty acid metabolism and cancer. Cell Metab. *18*, 153–161.

DeBerardinis, R.J., and Thompson, C.B. (2012). Cellular metabolism and disease: What do metabolic outliers teach us? Cell *148*, 1132–1144.

Dibble, C.C., and Manning, B.D. (2013). Signal integration by mTORC1 coordinates nutrient input with biosynthetic output. Nat. Cell Biol. *15*, 555–564.

Duan, S., Skaar, J.R., Kuchay, S., Toschi, A., Kanarek, N., Ben-Neriah, Y., and Pagano, M. (2011). mTOR generates an auto-amplification loop by triggering the βTrCP- and CK1α-dependent degradation of DEPTOR. Mol. Cell *44*, 317–324.

Düvel, K., Yecies, J.L., Menon, S., Raman, P., Lipovsky, A.I., Souza, A.L., Triantafellow, E., Ma, Q., Gorski, R., Cleaver, S., et al. (2010). Activation of a metabolic gene regulatory network downstream of mTOR complex 1. Mol. Cell *39*, 171–183.

Fabian, M.R., Sonenberg, N., and Filipowicz, W. (2010). Regulation of mRNA translation and stability by microRNAs. Annu. Rev. Biochem. *79*, 351–379.

Flotow, H., Graves, P.R., Wang, A.Q., Fiol, C.J., Roeske, R.W., and Roach, P.J. (1990). Phosphate groups as substrate determinants for casein kinase I action. J. Biol. Chem. *265*, 14264–14269.

Fu, X.-D., and Ares, M., Jr. (2014). Context-dependent control of alternative splicing by RNA-binding proteins. Nat. Rev. Genet. *15*, 689–701.

Fukuhara, T., Hosoya, T., Shimizu, S., Sumi, K., Oshiro, T., Yoshinaka, Y., Suzuki, M., Yamamoto, N., Herzenberg, L.A., Herzenberg, L.A., and Hagiwara, M. (2006). Utilization of host SR protein kinases and RNA-splicing machinery during viral replication. Proc. Natl. Acad. Sci. USA *103*, 11329–11333.

Gammons, M.V., Lucas, R., Dean, R., Coupland, S.E., Oltean, S., and Bates, D.O. (2014). Targeting SRPK1 to control VEGF-mediated tumour angiogenesis in metastatic melanoma. Br. J. Cancer *111*, 477–485.

Gao, D., Inuzuka, H., Tan, M.-K.M., Fukushima, H., Locasale, J.W., Liu, P., Wan, L., Zhai, B., Chin, Y.R., Shaik, S., et al. (2011). mTOR drives its own activation via SCF(βTrCP)-dependent degradation of the mTOR inhibitor DEPTOR. Mol. Cell *44*, 290–303.

Ghosh, G., and Adams, J.A. (2011). Phosphorylation mechanism and structure of serine-arginine protein kinases. FEBS J. *278*, 587–597.

Gilbert, W.V., Bell, T.A., and Schaening, C. (2016). Messenger RNA modifications: Form, distribution, and function. Science *80* (352), 1408–1412.

Gomes, A.P., and Blenis, J. (2015). A nexus for cellular homeostasis: The interplay between metabolic and signal transduction pathways. Curr. Opin. Biotechnol. *34*, 110–117.

Gonzalez Herrera, K.N., Lee, J., and Haigis, M.C. (2015). Intersections between mitochondrial sirtuin signaling and tumor cell metabolism. Crit. Rev. Biochem. Mol. Biol. *50*, 242–255.

Gout, S., Brambilla, E., Boudria, A., Drissi, R., Lantuejoul, S., Gazzeri, S., and Eymin, B. (2012). Abnormal expression of the pre-mRNA splicing regulators SRSF1, SRSF2, SRPK1 and SRPK2 in non small cell lung carcinoma. PLoS ONE *7*, e46539.

Han, J., Li, E., Chen, L., Zhang, Y., Wei, F., Liu, J., Deng, H., and Wang, Y. (2015). The CREB coactivator CRTC2 controls hepatic lipid metabolism by regulating SREBP1. Nature *524*, 243–246.

Horton, J.D., Goldstein, J.L., and Brown, M.S. (2002). SREBPs: Activators of the complete program of cholesterol and fatty acid synthesis in the liver. J. Clin. Invest. *109*, 1125–1131.

Howe, S.R., Gottardis, M.M., Everitt, J.I., Goldsworthy, T.L., Wolf, D.C., and Walker, C. (1995). Rodent model of reproductive tract leiomyomata. Establishment and characterization of tumor-derived cell lines. Am. J. Pathol. *146*, 1568–1579.

Hsu, P.P., Kang, S.A., Rameseder, J., Zhang, Y., Ottina, K.A., Lim, D., Peterson, T.R., Choi, Y., Gray, N.S., Yaffe, M.B., et al. (2011). The mTOR-regulated phosphoproteome reveals a mechanism of mTORC1-mediated inhibition of growth factor signaling. Science *332*, 1317–1322.

Isken, O., and Maquat, L.E. (2008). The multiple lives of NMD factors: Balancing roles in gene and genome regulation. Nat. Rev. Genet. *9*, 699–712.

Jang, S.-W., Yang, S.-J., Ehlén, A., Dong, S., Khoury, H., Chen, J., Persson, J.L., and Ye, K. (2008). Serine/arginine protein-specific kinase 2 promotes leukemia cell proliferation by phosphorylating acinus and regulating cyclin A1. Cancer Res. *68*, 4559–4570.

Jang, S.-W., Liu, X., Fu, H., Rees, H., Yepes, M., Levey, A., and Ye, K. (2009). Interaction of Akt-phosphorylated SRPK2 with 14-3-3 mediates cell cycle and cell death in neurons. J. Biol. Chem. *284*, 24512–24525.

Kamphorst, J.J., Cross, J.R., Fan, J., de Stanchina, E., Mathew, R., White, E.P., Thompson, C.B., and Rabinowitz, J.D. (2013). Hypoxic and Ras-transformed cells support growth by scavenging unsaturated fatty acids from lysophospholipids. Proc. Natl. Acad. Sci. USA *110*, 8882–8887.

Kohtz, J.D., Jamison, S.F., Will, C.L., Zuo, P., Lührmann, R., Garcia-Blanco, M.A., and Manley, J.L. (1994). Protein-protein interactions and 5′-splice-site recognition in mammalian mRNA precursors. Nature *368*, 119–124.

Kosugi, S., Hasebe, M., Tomita, M., and Yanagawa, H. (2009). Systematic identification of cell cycle-dependent yeast nucleocytoplasmic shuttling proteins by prediction of composite motifs. Proc. Natl. Acad. Sci. USA *106*, 10171–10176.

Lee, Y., and Rio, D.C. (2015). Mechanisms and Regulation of Alternative Pre-mRNA Splicing. Annu. Rev. Biochem. *84*, 291–323.

Li, S., Brown, M.S., and Goldstein, J.L. (2010). Bifurcation of insulin signaling pathway in rat liver: mTORC1 required for stimulation of lipogenesis, but not inhibition of gluconeogenesis. Proc. Natl. Acad. Sci. USA *107*, 3441–3446.

Lindsley, C.W. (2010). The Akt/PKB family of protein kinases: a review of small molecule inhibitors and progress towards target validation: a 2009 update. Curr. Top. Med. Chem *10*, 458–477.

Ma, X.M., and Blenis, J. (2009). Molecular mechanisms of mTOR-mediated translational control. Nat. Rev. Mol. Cell Biol. *10*, 307–318.

Manning, B.D., and Toker, A. (2017). AKT/PKB signaling: Navigating the network. Cell *169*, 381–405.

Mendoza, M.C., Er, E.E., and Blenis, J. (2011). The Ras-ERK and PI3K-mTOR pathways: Cross-talk and compensation. Trends Biochem. Sci. *36*, 320–328.

Menendez, J.A., and Lupu, R. (2007). Fatty acid synthase and the lipogenic phenotype in cancer pathogenesis. Nat. Rev. Cancer *7*, 763–777.

Menon, S., and Manning, B.D. (2008). Common corruption of the mTOR signaling network in human tumors. Oncogene *27* (*Suppl 2*), S43–S51.

Moore, M.J., and Proudfoot, N.J. (2009). Pre-mRNA processing reaches back to transcription and ahead to translation. Cell *136*, 688–700.

Nardozzi, J.D., Lott, K., and Cingolani, G. (2010). Phosphorylation meets nuclear import: A review. Cell Commun. Signal. *8*, 32.

Owen, J.L., Zhang, Y., Bae, S.-H., Farooqi, M.S., Liang, G., Hammer, R.E., Goldstein, J.L., and Brown, M.S. (2012). Insulin stimulation of SREBP-1c processing in transgenic rat hepatocytes requires p70 S6-kinase. Proc. Natl. Acad. Sci. USA *109*, 16184–16189.

Park, S.G., Ewalt, K.L., and Kim, S. (2005). Functional expansion of aminoacyl-tRNA synthetases and their interacting factors: New perspectives on housekeepers. Trends Biochem. Sci. *30*, 569–574.

Pascual, G., Avgustinova, A., Mejetta, S., Martín, M., Castellanos, A., Attolini, C.S.-O., Berenguer, A., Prats, N., Toll, A., Hueto, J.A., et al. (2017). Targeting metastasis-initiating cells through the fatty acid receptor CD36. Nature *541*, 41–45.

Paz, I., Kosti, I., Ares, M., Jr., Cline, M., and Mandel-Gutfreund, Y. (2014). RBPmap: A web server for mapping binding sites of RNA-binding proteins. Nucleic Acids Res. *42*, W361–W367.

Pearce, L.R., Komander, D., and Alessi, D.R. (2010a). The nuts and bolts of AGC protein kinases. Nat. Rev. Mol. Cell Biol. *11*, 9–22.

Pearce, L.R., Alton, G.R., Richter, D.T., Kath, J.C., Lingardo, L., Chapman, J., Hwang, C., and Alessi, D.R. (2010b). Characterization of PF-4708671, a novel and highly specific inhibitor of p70 ribosomal S6 kinase (S6K1). Biochem. J. *431*, 245–255.

Peterson, T.R., Sengupta, S.S., Harris, T.E., Carmack, A.E., Kang, S.A., Balderas, E., Guertin, D.A., Madden, K.L., Carpenter, A.E., Finck, B.N., and Sabatini, D.M. (2011). mTOR complex 1 regulates lipin 1 localization to control the SREBP pathway. Cell *146*, 408–420.

Ricoult, S.J.H., Yecies, J.L., Ben-Sahra, I., and Manning, B.D. (2016). Oncogenic PI3K and K-Ras stimulate de novo lipid synthesis through mTORC1 and SREBP. Oncogene *35*, 1250–1260.

Rittinger, K., Budman, J., Xu, J., Volinia, S., Cantley, L.C., Smerdon, S.J., Gamblin, S.J., and Yaffe, M.B. (1999). Structural analysis of 14-3-3 phosphopeptide complexes identifies a dual role for the nuclear export signal of 14-3-3 in ligand binding. Mol. Cell *4*, 153–166.

Robitaille, A.M., Christen, S., Shimobayashi, M., Cornu, M., Fava, L.L., Moes, S., Prescianotto-Baschong, C., Sauer, U., Jenoe, P., and Hall, M.N. (2013). Quantitative phosphoproteomics reveal mTORC1 activates de novo pyrimidine synthesis. Science *339*, 1320–1323.

Sanjana, N.E., Shalem, O., and Zhang, F. (2014). Improved vectors and genome-wide libraries for CRISPR screening. Nat. Methods *11*, 783–784.

Saxton, R.A., and Sabatini, D.M. (2017). mTOR Signaling in Growth, Metabolism, and Disease. Cell *168*, 960–976.

Schalm, S.S., and Blenis, J. (2002). Identification of a conserved motif required for mTOR signaling. Curr. Biol. *12*, 632–639.

Selwan, E.M., Finicle, B.T., Kim, S.M., and Edinger, A.L. (2016). Attacking the supply wagons to starve cancer cells to death. FEBS Lett. *590*, 885–907.

Shimobayashi, M., and Hall, M.N. (2014). Making new contacts: The mTOR network in metabolism and signalling crosstalk. Nat. Rev. Mol. Cell Biol. *15*, 155–162.

Siroky, B.J., Yin, H., Babcock, J.T., Lu, L., Hellmann, A.R., Dixon, B.P., Quilliam, L.A., and Bissler, J.J. (2012). Human TSC-associated renal angiomyolipoma cells are hypersensitive to ER stress. Am. J. Physiol. Renal Physiol. *303*, F831–F844.

Tani, H., and Akimitsu, N. (2012). Genome-wide technology for determining RNA stability in mammalian cells: Historical perspective and recent advantages based on modified nucleotide labeling. RNA Biol. *9*, 1233–1238.

Thoreen, C.C., Kang, S.A., Chang, J.W., Liu, Q., Zhang, J., Gao, Y., Reichling, L.J., Sim, T., Sabatini, D.M., and Gray, N.S. (2009). An ATP-competitive mammalian target of rapamycin inhibitor reveals rapamycin-resistant functions of mTORC1. J. Biol. Chem. *284*, 8023–8032.

Tyanova, S., Temu, T., Sinitcyn, P., Carlson, A., Hein, M.Y., Geiger, T., Mann, M., and Cox, J. (2016). The Perseus computational platform for comprehensive analysis of (prote)omics data. Nat. Methods *13*, 731–740.

Vander Heiden, M.G., Cantley, L.C., and Thompson, C.B. (2009). Understanding the Warburg effect: The metabolic requirements of cell proliferation. Science *324*, 1029–1033.

Wang, H.Y., Lin, W., Dyck, J.A., Yeakley, J.M., Songyang, Z., Cantley, L.C., and Fu, X.D. (1998). SRPK2: A differentially expressed SR protein-specific kinase involved in mediating the interaction and localization of pre-mRNA splicing factors in mammalian cells. J. Cell Biol. *140*, 737–750.

Wang, J., Wu, H.-F., Shen, W., Xu, D.-Y., Ruan, T.-Y., Tao, G.-Q., and Lu, P.-H. (2016). SRPK2 promotes the growth and migration of the colon cancer cells. Gene *586*, 41–47.

Yu, J., Astrinidis, A., Howard, S., and Henske, E.P. (2004). Estradiol and tamoxifen stimulate LAM-associated angiomyolipoma cell growth and activate both genomic and nongenomic signaling pathways. Am. J. Physiol. Lung Cell. Mol. Physiol. *286*, L694–L700.

Yu, J.J., Robb, V.A., Morrison, T.A., Ariazi, E.A., Karbowniczek, M., Astrinidis, A., Wang, C., Hernandez-Cuebas, L., Seeholzer, L.F., Nicolas, E., et al. (2009). Estrogen promotes the survival and pulmonary metastasis of tuberin-null cells. Proc. Natl. Acad. Sci. USA *106*, 2635–2640.

Yu, Y., Yoon, S.-O., Poulogiannis, G., Yang, Q., Ma, X.M., Villén, J., Kubica, N., Hoffman, G.R., Cantley, L.C., Gygi, S.P., and Blenis, J. (2011). Phosphoproteomic analysis identifies Grb10 as an mTORC1 substrate that negatively regulates insulin signaling. Science *332*, 1322–1326.

Zhang, H., Cicchetti, G., Onda, H., Koon, H.B., Asrican, K., Bajraszewski, N., Vazquez, F., Carpenter, C.L., and Kwiatkowski, D.J. (2003). Loss of Tsc1/Tsc2 activates mTOR and disrupts PI3K-Akt signaling through downregulation of PDGFR. J. Clin. Invest. *112*, 1223–1233.

Zhang, J., Yang, P.L., and Gray, N.S. (2009). Targeting cancer with small molecule kinase inhibitors. Nat. Rev. Cancer *9*, 28–39.

Zhang, Y., Nicholatos, J., Dreier, J.R., Ricoult, S.J.H., Widenmaier, S.B., Hotamisligil, G.S., Kwiatkowski, D.J., and Manning, B.D. (2014). Coordinated regulation of protein synthesis and degradation by mTORC1. Nature *513*, 440–443.

Zheng, Y., Yin, H., Boeglin, W.E., Elias, P.M., Crumrine, D., Beier, D.R., and Brash, A.R. (2011). Lipoxygenases mediate the effect of essential fatty acid in skin barrier formation: A proposed role in releasing omega-hydroxyceramide for construction of the corneocyte lipid envelope. J. Biol. Chem. *286*, 24046–24056.

Zhou, Z., Qiu, J., Liu, W., Zhou, Y., Plocinik, R.M., Li, H., Hu, Q., Ghosh, G., Adams, J.A., Rosenfeld, M.G., and Fu, X.D. (2012). The Akt-SRPK-SR axis constitutes a major pathway in transducing EGF signaling to regulate alternative splicing in the nucleus. Mol. Cell *47*, 422–433.

STAR★METHODS

KEY RESOURCES TABLE

REAGENT or RESOURCE	SOURCE	IDENTIFIER
Antibodies		
Rabbit polyclonal anti-pSRPK2(S494)	This paper	N/A
Rabbit polyclonal anti-pSRPK2(S497)	This paper	N/A
Rabbit polyclonal anti-pSRPK2(S494/S497)	This paper	N/A
Mouse monoclonal anti-SRPK1	BD Biosciences	Cat#BD611072; RRID: AB_398385
Mouse monoclonal anti-SRPK2	BD Biosciences	Cat#BD611118; RRID: AB_398429
Rabbit polyclonal anti-ACLY	Cell Signaling Technology	Cat#4332; RRID: AB_2223744
Rabbit monoclonal anti-FASN	Cell Signaling Technology	Cat#3180; RRID: AB_2100796
Rabbit polyclonal anti-SCD1	Cell Signaling Technology	Cat#2438; RRID: AB_823634
Mouse monoclonal anti-S6	Cell Signaling Technology	Cat#2317; RRID: AB_2238583
Rabbit polyclonal anti-pS6(S235/S236)	Cell Signaling Technology	Cat#2211; RRID: AB_331679
Rabbit monoclonal anti-pS6(S240/S244)	Cell Signaling Technology	Cat#5364; RRID: AB_10694233
Rabbit monoclonal anti-S6K1	Cell Signaling Technology	Cat#2708; RRID: AB_390722
Rabbit monoclonal anti-pS6K1(T389)	Cell Signaling Technology	Cat#9234; RRID: AB_2269803
Rabbit monoclonal anti-TSC2	Cell Signaling Technology	Cat#4308; RRID: AB_10547134
Rabbit monoclonal anti-V5	Cell Signaling Technology	Cat#13202; RRID: AB_2687461
Rabbit polyclonal anti-ACSS2	Sigma-Aldrich	Cat#HPA004141; RRID: AB_1078094
Mouse monoclonal anti-GAPDH	Sigma-Aldrich	Cat#G8795; RRID: AB_1078991
Rabbit monoclonal anti-FDFT1	Abcam	Cat#ab109723; RRID: AB_10859772
Mouse monoclonal anti-SRSF1	Santa Cruz	Cat#sc-33652; RRID: AB_628248
Goat polyclonal anti-ACTIN	Santa Cruz	Cat#sc-1615; RRID: AB_630835
Rabbit polyclonal anti-GST	Santa Cruz	Cat#sc-459; RRID: AB_631586
Goat polyclonal anti-LAMIN A/C	Santa Cruz	Cat#sc-6215; RRID: AB_648152
Rabbit polyclonal anti-SREBP1	Santa Cruz	Cat#sc-8984; RRID: AB_2194223
Mouse monoclonal anti-HA	Covance	Cat#MMS-101P; RRID: AB_2314672
Mouse monoclonal anti-U1-70k	Synaptic Systems	Cat#203-011; RRID: AB_887903
Mouse monoclonal anti-pSR proteins (mAB1H4)	Invitrogen	Cat#33-9400; RRID: AB_87195
Bacterial and Virus Strains		
E. coli BL21	New England Biolabs	Cat#C2527
Chemicals, Peptides, and Recombinant Proteins		
Insulin	Sigma-Aldrich	Cat#I9278
Rapamycin	Sigma-Aldrich	Cat#R8781
Rapamycin	Calbiochem	Cat#553210
PF4708671	Sigma-Aldrich	Cat#PZ0143
Actinomycin D	Sigma-Aldrich	Cat#A1410
Torin1	Tocris Bioscience	Cat#4247
MK2206	Cayman Chemical	Cat#11593
SRPIN340	Selleck Chemicals	Cat#S7270
DNase I	QIAGEN	Cat#79254
DNase I	Sigma-Aldrich	Cat#AMPD1
[1-^{14}C]-Acetate	Perkin Elmer	Cat#NEC084H001MC
[γ-^{32}P]-ATP	Perkin Elmer	Cat#NEG035C001MC

(*Continued on next page*)

Continued

REAGENT or RESOURCE	SOURCE	IDENTIFIER
13(S)-hydroxyoctadecadienoic acid [13(S)-HODE]	Cayman Chemicals	Cat#38610
[U-^{13}C]-glucose	Cambridge Isotope Laboratories	Cat#CLM-1396
Lipoprotein, low density from human plasma	Sigma-Aldrich	Cat#L7914
Oleic acid-albumin	Sigma-Aldrich	Cat#O3008
Fatty acid-free albumin	Sigma-Aldrich	Cat#A8806
Dialyzed FBS	Sigma-Aldrich	Cat#F0392
Lipoprotein-deficient serum	Alfa Aesar	Cat#BT-907
Lipoprotein-deficient serum	Intracel	Cat#RP-054
Triiodothyronine	Sigma-Aldrich	Cat#T2752
Vasopressin	Sigma-Aldrich	Cat#V0377
Hydrocortisone	Sigma-Aldrich	Cat#H4001
Sodium selenite	Fisher	Cat#CB40201
Cholesterol	Sigma-Aldrich	Cat#C3045
EGF	Fisher	Cat#CB40001
Transferrin	Sigma-Aldrich	Cat#T0665
Ferrous sulfate	Fisher	Cat#I146
PhosSTOP	Roche	Cat#04906837001
RNase inhibitor	Invitrogen	Cat#10777019
Anti-V5 agarose affinity gel	Sigma-Aldrich	Cat#A7345
V5 peptide	Sigma-Aldrich	Cat#V7754
Protein A/G magnetic beads	Thermo Fisher Scientific	Cat#88802
Protein A Sepharose beads	GE Healthcare Life Sciences	Cat#17528001
Protein G Sepharose beads	GE Healthcare Life Sciences	Cat#17061801
Glutathione Sepharose 4B	GE Healthcare Life Sciences	Cat#17075601
Proteinase K	New England Biolabs	Cat#P8107
SE. Cell Line 4D-Nucleofector X Kit	Lonza	Cat#V4XC-1032
Lipofectamine RNAiMAX reagent	Invitrogen	Cat#13778075
Lipofectamine 2000 reagent	Invitrogen	Cat#11668500
FuGENE HD transfection reagent	Promega	Cat#E2311
Calf intestinal alkaline phosphatase (CIAP)	New England Biolabs	Cat#M0290S
Isopropyl beta-D-1-thiogalactopyranoside (IPTG)	Sigma-Aldrich	Cat#I6758
Reduced glutathione	Thermo Fisher	Cat#78259
GST-CK1 (purified protein)	EMD Millipore	Cat#14-520
Hoechst 33258, Pentahydrate (bis-Benzimide)	Thermo Fisher	Cat#H3569
Critical Commercial Assays		
RNeasy Mini Kit	QIAGEN	Cat#74106
PureLink RNA Mini kit	Ambion	Cat#12183018A
iScript cDNA synthesis kit	Bio-rad	Cat#170-8891BUN
GeneChip whole transcript (WT) plus reagent kit	Affymetrix	Cat#902281
GeneChip WT terminal labeling kit	Affymetrix	Cat#900671
Imprint RNA Immunoprecipitation Kit	Sigma-Aldrich	Cat#RIP SIGMA
LightSwitch dual assay kit (promoter assay)	Active Motif	Cat#32035
Gateway BP clonase II enzyme mix	Invitrogen	Cat#11789
Gateway LR clonase II enzyme mix	Invitrogen	Cat#11791

(*Continued on next page*)

Continued

REAGENT or RESOURCE	SOURCE	IDENTIFIER
QuickChange site-directed mutagenesis kit	Strategene	Cat#200521
NE-PER kit (nuclear-cytoplasmic fractionation)	Thermo Fisher Scientific	Cat#78835
Deposited Data		
Raw and analyzed whole transcriptome array data	This paper	GEO: GSE104335
Experimental Models: Cell Lines		
Human renal angiomyolipoma-derived LAM 621-101 (*TSC2*−/−)	Drs. Jane Yu and Elizabeth Henske	Yu et al., 2004
Rat uterine leiomyoma-derived ELT3 (*Tsc2*−/−)	Dr. Cheryl Walker	Howe et al., 1995
Mouse embryonic fibroblasts (*Tsc2*−/−)	Dr. David Kwiatkowski	Zhang et al., 2003
HEK293E	Dr. John Blenis	N/A
HEK293T	GenHunter	Cat#Q401
RT4	ATCC	Cat#HTB-2; RRID: CVCL_0036
MCF7	ATCC	Cat#HTB-22; RRID: CVCL_0031
DLD1	ATCC	Cat#CCL-221; RRID: CVCL_0248
A549	ATCC	Cat#CCL-185; RRID: CVCL_0023
mAb104	ATCC	Cat#CRL-2067; RRID: CVCL_G668
Experimental Models: Organisms/Strains		
Female nude CD-1 mice	Charles River	Cat#CD1-*Foxn1*^{nu}
Female NOD/SCID-gamma mice	Jackson Lab	Cat#005557
Female CB17-SCID mice	Taconic	Cat#CB17SC-F
Oligonucleotides		
siRNA negative control (siNTC)	QIAGEN	Cat#1027281
siRNA (Human S6K1, Importin β1, SRSF1, SRSF2, SRSF3, SRSF4, SRSF5, UPF1)	Dharmacon/GE	ON-TARGETplus SMARTpool siRNA
siRNA (Human SRPK1)	Sigma-Aldrich	SASI_Hs01_00120806
siRNA (Human SRPK1)	Sigma-Aldrich	SASI_Hs01_00120807
siRNA (Human SRPK1)	Sigma-Aldrich	SASI_Hs01_00120808
siRNA (Human SRPK2)	Sigma-Aldrich	SASI_Hs01_00057789
siRNA (Human SRPK2)	Sigma-Aldrich	SASI_Hs01_00057790
siRNA (Human SRPK2)	Sigma-Aldrich	SASI_Hs01_00057791
siRNA (Human SREBP1)	Sigma-Aldrich	SASI_Hs01_00051828
siRNA (Human SREBP1)	Sigma-Aldrich	SASI_Hs01_00051829
siRNA (Human SREBP1)	Sigma-Aldrich	SASI_Hs01_00051830
siRNA (Human SREBP2)	Sigma-Aldrich	SASI_Hs01_00075424
siRNA (Human SREBP2)	Sigma-Aldrich	SASI_Hs01_00075425
siRNA (Human SREBP2)	Sigma-Aldrich	SASI_Hs01_00075426
siRNA (Human U1-70k/SNRNP70)	Sigma-Aldrich	SASI_Hs02_00335028
siRNA (Human U1-70k/SNRNP70)	Sigma-Aldrich	SASI_Hs01_00165101
pLKO.1-puro-shGFP	Broad Institute	TRCN0000072181
pLKO.1-puro-shSRPK2#6	Broad Institute	TRCN0000006274
pLKO.1-puro-shSRPK2#10	Broad Institute	TRCN0000006278
sgRNA targeting sequence (Human SRPK2): GCATTATACGGAGACAGCCT	This paper	N/A
sgRNA targeting sequence (Human SRPK2): GGATCCGCGGAATGCAGATA	This paper	N/A

(*Continued on next page*)

Continued

REAGENT or RESOURCE	SOURCE	IDENTIFIER
sgRNA targeting sequence (Human SRPK2): GACGCGTCAGTACCGCTCCA	This paper	N/A
Primers for qPCR analysis, see Table S3	This paper	N/A
Recombinant DNA		
FDFT1 promoter construct	SwitchGear Genomics	Cat#S714149
SCD1 promoter construct	SwitchGear Genomics	Cat#S714484
ACLY promoter construct	SwitchGear Genomics	Cat#S715276
ACSS2 promoter construct	SwitchGear Genomics	Cat#S715263
Cypridina TK control promoter construct	SwitchGear Genomics	Cat#SN0322S
Retroviral packaging and envelope plasmids	Dr. Robert Weinberg	N/A
Lentiviral packaging and envelope plasmids	Dr. David Baltimore	N/A
pKH3-SRPK2-WT, S494A, K110M	This paper	N/A
pLNCX-SRPK2-WT, S494A, S497A, S494A/S497A,	This paper	N/A
pGEX-2T-SRPK2 WT, S494A, S494D, S494A/S497A (454-521 amino acids)	This paper	N/A
pLX304-SRSF1-V5	Harvard plasmid	Cat#HsCD00420441
pCMV-SPORT6-mouse Srpk2	Harvard plasmid	Cat#MmCD00316576
pDONR223-mouse Srpk2	This paper	N/A
pLenti-Blast-mouse Srpk2-WT, S488A/S491A	This paper	N/A
pKH3-S6K1-F5A/T389E/R3A	Dr. John Blenis	Schalm and Blenis, 2002
lentiCRISPRv2 vector	Dr. Feng Zhang	Sanjana et al., 2014
Software and Algorithms		
Expression console software	Affymetrix	Affymetrix
Transcriptome analysis console software	Affymetrix	Affymetrix
Agilent OpenLAB CDS ChemStation	Agilent	Agilent
MAVEN software	Kamphorst et al., 2013	http://genomics-pubs.princeton.edu/mzroll/index.php
Maxquant analysis platform	Tyanova et al., 2016	http://www.coxdocs.org/doku.php?id=maxquant:start
Perseus	Tyanova et al., 2016	http://www.coxdocs.org/doku.php?id=perseus:start
Andromeda algorithm	Tyanova et al., 2016	http://www.coxdocs.org/doku.php?id=maxquant:start
Adobe Photoshop	Adobe	Adobe
Odyssey imaging system	LI-COR Biosciences	LI-COR Biosciences
MetaMorph software	Molecular Devices	Molecular Devices
DAVID	Open source	https://david.ncifcrf.gov/
WebGestalt	Open source	http://www.webgestalt.org/
RBPmap	Open source	http://rbpmap.technion.ac.il/
NLS-mapper	Open source	http://nls-mapper.iab.keio.ac.jp/

CONTACT FOR REAGENT AND RESOURCE SHARING

Further information and requests for resources and reagents should be directed to and will be fulfilled by the Lead Contact, John Blenis (job2064@med.cornell.edu).

EXPERIMENTAL MODEL AND SUBJECT DETAILS

Cell lines

RT4, MCF7, DLD1, A549, and mAb104 cells were obtained from ATCC. HEK293T cells were obtained from GenHunter. Human renal angiomyolipoma-derived LAM 621-101 (*TSC2*−/−) cell line immortalized by HPV E6/E7 and hTERT was described before (Yu et al., 2004). Eker rat uterine leiomyoma-derived ELT3 (*Tsc2*−/−) cell line was provided by Cheryl Walker (Texas A & M University) (Howe et al., 1995) and used to generate ELT3-luciferase cell line stably expressing luciferase as previously described (Yu et al., 2009). *Tsc2*−/− mouse embryonic fibroblasts (MEFs) were provided by David Kwiatkowski (Harvard Medical School) (Zhang et al., 2003). Cells were grown in the following media at 37°C with 5% CO_2 unless otherwise stated. HEK293E, HEK293T, RT4, and *Tsc2*−/− MEFs were cultured in DMEM with 10% FBS. MCF7, DLD1, and A549 cells were cultured in RPMI with 10% FBS. mAb104 cells were cultured in Iscove's modified Dulbecco's medium (IMDM) with 20% FBS. LAM 621-101 and ELT3 cells were cultured in IIA complete media (DMEM/F12, 10% FBS, 1 nM triiodothyronine, 10 μU/mL vasopressin, 200 nM hydrocortisone, 50 nM sodium selenite, 10 nM cholesterol, 20 ng/mL EGF, 25 μg/mL insulin, 10 μg/mL transferrin, and 1.6 μM ferrous sulfate) (Yu et al., 2004; Yu et al., 2009).

Mice

All animal work was performed in accordance with protocols approved by the University of Cincinnati Standing Committees on Animals. 6-8 week-old female nude CD-1 mice (Charles River), NOD/SCID-gamma mice (Jackson Lab), and CB17-scid mice (Taconic) were used.

Microbe strains

E. coli BL21 (New England Biolabs) was grown at 28°C in 2x YTA medium for protein purification.

METHODS DETAILS

Antibodies and small molecule inhibitors

Cell Signaling Technology custom developed the pSRPK2(S494), pSRPK2(S497), and pSRPK2(S494/S497) antibodies for this study. Antibodies were obtained from following sources: SRPK1 and SRPK2 from BD Biosciences; ACLY, FASN, SCD1, S6, pS6(S235/S236), pS6(S240/S244), S6K1, pS6K1(T389), TSC2, and V5 from Cell Signaling Technology; ACSS2 and GAPDH from Sigma-Aldrich; FDFT1 from Abcam; SRSF1, ACTIN, GST, LAMIN A/C, and SREBP1 from Santa Cruz; HA from Covance; U1-70k from Synaptic Systems. Monoclonal antibody for the phosphorylated SR proteins was generated from the mAb104 hybridoma cell line (ATCC) (Figures 3B and 3H) or purchased from invitrogen (mAB1H4) (Figure 5G). Reagents were obtained from following sources: Insulin, rapamycin, PF4708671, and actinomycin D from Sigma-Aldrich; Torin1 from Tocris Bioscience; rapamycin from Calbiochem; MK2206 from Cayman Chemical; SRPIN340 from Selleck Chemicals and Milstein Chemistry Core Facility (Weill Cornell Medicine).

Gene expression analysis and measurement of mRNA stability

RNA was isolated using RNeasy Mini Kit (QIAGEN) or PureLink RNA Mini kit (Ambion) and treated with DNase I (QIAGEN or Sigma-Aldrich) according to the manufacturers' instructions. After reverse-transcription of 500-1,000 ng RNA (iScript cDNA synthesis kit, Bio-rad), the resulting cDNA was diluted in nuclease-free water (1:5) followed by quantitative real-time PCR (qPCR) using QuantStudio 6 Flex (Applied Biosystems). Gene expression levels were normalized to the expression level of the housekeeping genes *ACTIN*, *TATA-binding protein* (*TBP*) or *Peptidylpropyl isomerase B* (*PPIB*). To measure mRNA stability, transcription was blocked by actinomycin D (5 μg/ml) treatment for 0, 2, and 4 hr. Reverse-transcription was performed using the same volume of RNA for all time points and the mRNA levels were measured by qPCR (Tani and Akimitsu, 2012).

Human whole transcriptome microarray

Total RNA was isolated using RNeasy Mini Kit (QIAGEN) and treated with DNase I (QIAGEN). Microarray was performed by the Translational Genomics Core at Partners HealthCare Personalized Medicine (MA, USA) according to the protocol from Affymetrix. Briefly, 100 ng total RNA was used to synthesize biotinylated cDNA using GeneChip whole transcript (WT) plus reagent kit. 5.5 μg cDNA was fragmented and labeled by terminal deoxynucleotidyl transferase (GeneChip WT terminal labeling kit). The resulting cDNA was hybridized to the Human Transcriptome 2.0 Array at 45°C for 16 hr. Array chips were washed and stained using GeneChip fluidics station 450, and scanned using GeneChip Scanner 3000 7G. Data were analyzed by Expression console (Affymetrix) and Transcriptome analysis console software (Affymetrix) according to the manufacturer's instruction.

HPLC analysis of *de novo* lipid synthesis

Cells in a 6-well plate were cultured in serum-free DMEM (5.5 mM glucose) overnight or for 24 hr (for drug treatment conditions), and labeled with [1-^{14}C]-acetate (2-8 μCi/well) (Perkin Elmer) for the last 6 hr. The cells were washed three times with PBS and lysed by methanol containing the internal standard 13(S)-hydroxyoctadecadienoic acid [13(S)-HODE] (2 μg/well) (Cayman Chemicals). Cell lysates were collected with a cell scraper and transferred to a glass vial. Lipids were extracted by addition of chloroform and water

(methanol:chroloform:water = 1:1:0.9, by volume). After centrifugation (800 rpm, 10 min), the lower phase was transferred to a new vial and evaporated under a stream of N_2. The lipids were then dissolved in methanol (1 mL), hydrolyzed by 0.5 mL of 1 N NaOH at room temperature for 2 hr, and re-extracted by addition of chloroform (2 mL), 1N HCl (0.5 mL), and water (2 mL). After centrifugation, the lower phase was transferred to a new vial. Samples were evaporated under a stream of N_2 and dissolved in 0.2 mL of hexane: isopropanol:acetic acid (100:3:0.02, by volume) for HPLC analysis. Samples were analyzed using an Agilent Zorbax Silica column (5 μm, 4.6x250 mm) with isocratic elution of hexane:isopropanol:acetic acid (100:3:0.02, by volume) at a flow rate of 1 mL/min over 12 min, on an Agilent 1260 Infinity binary system with a Diode array detector coupled to a Perkin-Elmer Radiometric 150TR detector (Zheng et al., 2011). The retention time of fatty acids and cholesterol was determined by standard lipids. Peak areas of radiolabeled fatty acids and cholesterol were integrated (Agilent OpenLAB CDS ChemStation) and normalized to that of 13(S)-HODE and cell number.

LC-MS analysis of saponified fatty acids

Extraction and LC-MS analysis of fatty acids were performed as previously described (Kamphorst et al., 2013). Briefly, cells in a 60-mm plate were supplemented with 17.5 mM [U-^{13}C]-glucose (Cambridge Isotope Laboratories) in DMEM/F12 with or without 10% dialyzed FBS (Sigma-Aldrich) or lipoprotein-deficient serum (Intracel or Alfa Aesar) for 48 hr. The cells were washed three times with PBS and lysed with 2 mL of 0.3 M KOH in 90% methanol. Cell lysates were collected with a cell scraper and transferred to a glass vial. Lipids were hydrolyzed at 80°C for 1 hr and formic acid (0.2 mL) was added for neutralization. The lipids were extracted twice by adding 2 mL of hexane and transferring the top layer to a new vial. Samples were evaporated under a stream of N_2 and dissolved in 0.1 mL of isopropanol:methanol (1:1, v/v) solution for LC-MS analysis (Stand-alone Orbitrap, Thermo Fisher). De novo synthesized fatty acids were determined based on the sum of all forms containing four or more labeled carbon atoms (fatty acids containing 2-labeled carbon atoms are made from elongation not *de novo* synthesis). Data analysis with MAVEN software and natural isotope correction were performed as previously described (Kamphorst et al., 2013).

Cell proliferation assay

Cells seeded on a 12-well plate (LAM 621-101, 2 × 10^3 cells; MCF7 and RT4, 2 × 10^4 cells) were grown in the media (LAM 621-101, DMEM/F12; MCF7, RPMI; RT4, DMEM) with 10% FBS or LPDS for 8 days. Lipoprotein (25 μg/ml), oleic acid-albumin (50 μM), or fatty acid-free albumin (25 μM) was supplemented to the media. Cristal violet staining was performed to visualize cells. Briefly, cells were fixed with 4% methanol-free formaldehyde (Polysciences) in PBS for 30 min and rinsed with PBS. The cells were incubated with 0.1% crystal violet solution (Sigma-Aldrich) for 30 min at room temperature. After rinsing five times with water, the plate was air-dried and scanned. Quantification was performed by densitometry analysis of images using Adobe Photoshop.

In vivo xenograft tumor assay

All animal work was performed in accordance with protocols approved by the University of Cincinnati Standing Committees on Animals. Female nude CD-1 mice (Charles River) (A549 cell line), NOD/SCID-gamma mice (Jackson Lab) (LAM 621-101 cell line), and CB17-scid mice (Taconic) (RT4 and ELT3-luciferase cell lines), 6 to 8 weeks of age, were used. 2x10^6 cells were subcutaneously inoculated into the posterior back regions of each mouse. Once the tumor is formed three to five weeks post inoculation, tumor length and width were measured using a digital caliper. Tumor volume was calculated using the formula: volume = (length × (width)^2/2). For the drug treatment experiment, mice were randomized into two groups after tumor formation and treated with either vehicle control (100 μL of 1% DMSO in PBS) or SRPIN340 (100 μL of 20 μg/ml; 1% DMSO in PBS) by daily peritumoral injection as previously described (Gammons et al., 2014). SRPIN340 was dissolved as 2 mg/ml in DMSO, and this stock solution was diluted 1:1,000 using PBS prior to inject. For the bioluminescent imaging of ELT3-luciferase tumors, luciferin (120 mg/kg, Xenogen) was intraperitoneally injected into the mouse 10 min prior to imaging. Bioluminescent signals were recorded using the Xenogen IVIS System and the total photon flux of tumors was analyzed as previously described (Yu et al., 2009).

Mass spectrometry analysis of SRSF1 interactome

HEK293E cells were transfected with empty vector (EV) or pLX304-SRSF1-V5. After 24 hr transfection, cells were treated with vehicle (DMSO) or Torin1 (250 nM) for additional 4 hr according to the three experimental conditions: EV+DMSO, SRSF1-V5+DMSO, and SRSF1-V5+Torin1. Cells were washed once with ice-cold PBS and disrupted on ice with lysis buffer (50 mM Tris-Cl buffer [pH 8], 150 mM NaCl, and 0.5% NP-40) supplemented with protease inhibitors (250 μM PMSF, 5 μg/ml pepstatin A, 10 μg/ml leupeptin, and 5 μg/ml aprotinin), phosphatase inhibitors (PhosSTOP, Roche), and RNase inhibitor (160 unit/ml). Lysates were homogenized by syringe. Cleared lysates were obtained by centrifugation at 15,000 rpm at 4°C for 30 min. For co-immunoprecipitation, lysates were incubated with anti-V5 agarose affinity gel (Sigma-Aldrich) at 4°C for 2.5 hr and washed three times with the lysis buffer. Immunoprecipitated proteins were analyzed by immunoblotting or further processed for the mass spectrometry (MS) analysis.

For MS analysis, the immunoprecipitated proteins were eluted from the beads by incubating with V5 peptide (Sigma-Aldrich) overnight at 4°C. Protein elutes were precipitated with trichloroacetic acid (TCA, 20% w/v), rinsed three times with acetone, and dried at room temperature. The pellets were re-suspended in 50 μL resuspension buffer (8 M urea, 50 mM ammonium bicarbonate, and 5 mM DTT) and subjected to reduction and alkylation reaction. Briefly, 15 mM iodoacetamide was added to each sample for 30 min in the dark at room temperature, followed by addition of another 5 mM DTT to quench the reaction. Samples were diluted to a final

concentration of 1 M urea, and then subsequently digested with LysC (room temperature, overnight) and trypsin (37°C, overnight) (each at a ratio of 1:125, enzyme:protein).

Samples were then labeled using triplex reductive dimethylation (Boersema et al., 2008). Labeling was done while the peptides were bound to the solid phase C18 resin in self-packed STAGE tip micro-columns. Stage tips were washed as previously described with methanol, acetonitrile (ACN, 70% v/v) and formic acid (FA, 1% v/v), and finally with 1% FA. Samples were acidified by adding 100% FA to a final concentration of 2% FA before loading. After sample loading, stage tips were washed with 1% FA and phosphate/citrate buffer (0.23 M sodium phosphate and 86.4 mM citric acid [pH 5.5]). At this point, the "light" solution for EV+DMSO (0.4% CH_2O and 60 mM $NaBH_3CN$)', "medium" solution for SRSF1-V5+DMSO (0.4% CD_2O and 60 mM $NaBH_3CN$), or "heavy" solution for SRSF1-V5+Torin1 (0.4% $^{13}CD_2O$ and 60 mM $NaBD_3CN$) was added twice on each stage tip to label the peptides. A final wash with 1% FA was performed prior to elution with 70% ACN and 1% FA. Samples were dried under vacuum, resuspended in 5% FA, and mixed together in equal amounts for analysis using an Orbitrap Fusion Mass Spectrometer (Thermo Fisher). Peptides were introduced into the mass spectrometer by nano-electrospray as they eluted off a self-packed 40 cm, 75 μm (ID) reverse-phase column packed with 1.8 μm, 120 Å pore size, SEPAX C18 resin. Peptides were separated with a gradient of 5%–25% buffer B (99.9% ACN, 0.1% FA) with a flow rate of 350 nl/min for 85 min. For each scan cycle, one high mass resolution full MS scan was acquired in the Orbitrap mass analyzer at a resolution of 120K, AGC value of 500,000, in a m/z scan range of 375-1,400, max acquisition time of 100 ms and up to 20 parent ions were chosen based on their intensity for collision induced dissociation (normalized collision energy = 35%) and MS/MS fragment ion scans at low mass resolution in the linear ion trap. Dynamic exclusion was enabled to exclude ions that had already been selected for MS/MS in the previous 40 s. Ions with a charge of +1 and those whose charge state could not be assigned were also excluded. All scans were collected in centroid mode.

Two biological replicates for each condition were processed and analyzed. All raw mass spectral data were processed using the Maxquant analysis platform and subsequent visualization and statistical analysis was done with Perseus (Tyanova et al., 2016). Spectra were searched using the Andromeda algorithm. Prior to run Maxquant, the following dynamic and fixed modifications were set: oxidation methionine and acetyl protein N-term (as dynamic), carbamidomethyl in cysteines (as fixed). Spectral matches were filtered to 1% false positive rate.

SILAC cell culture and mass spectrometry analysis of phosphorylated proteins

Sample preparation for the stable isotope labeling with amino acids in cell culture (SILAC) experiments and LC-MS/MS analysis were previously described (Yu et al., 2011). Briefly, *Tsc2*−/− MEFs were grown in light ($[^{12}C_6{}^{14}N_2]$-Lys, $[^{12}C_6{}^{14}N_4]$-Arg) or heavy ($[^{13}C_6{}^{15}N_2]$-Lys, $[^{13}C_6{}^{15}N_4]$-Arg) (Cambridge Isotope Laboratories) DMEM supplemented with 10% dialyzed FBS. Cells were serum starved for 17 hr and treated with vehicle or rapamycin (20 nM) for 2 hr. Cells were lysed and digested with trypsin, and the phosphopeptides were enriched by SCX-IMAC method. Samples were analyzed by LTQ-Orbitrap mass spectrometer (Thermo Fisher) as previously described (Yu et al., 2011).

RNA-protein immunoprecipitation (RNA-IP)

RNA-protein immunoprecipitation was performed using Imprint RNA immunoprepitation (RIP) kit (Sigma-Aldrich) according to the manufacturer's protocol. Cells on a 15-cm plate were washed twice with ice-cold PBS and harvested into Eppendorf tube. Cells were collected by centrifugation at 3,000 rpm at 4°C for 5 min. Cell pellets were re-suspended with 100 μL of strong lysis buffer (RIP kit) supplemented with protease inhibitors (protease inhibitor cocktail, 1 μL) and RNase inhibitor (160 unit/mL) and incubated on ice for 15 min. Cell lysates were snap-frozen in liquid nitrogen and thawed on ice.

To prepare antibody-prebound beads, 5 μg of mouse IgG (EMD Millipore) or anti-SRSF1 antibody (Santa Cruz) was conjugated to the 50 μL protein A/G magnetic beads (Thermo Fisher). Cell lysates and the antibody-prebound beads were incubated in 1 mL RIP buffer at 4°C for 3 hr. Beads were washed and RNA was eluted by incubating with 150 μL RIP buffer containing 1% SDS and 1.2 mg/mL proteinase K (New England Biolabs) at 55°C for 30 min. The eluted RNA was further purified by phenonol/chroloform extraction and precipitated with ammonium acetate and ethanol. Input and immunoprecipitated RNAs were treated with DNase I (Sigma-Aldrich) and reverse-transcribed (iScript cDNA synthesis kit, Bio-rad), and the resulting cDNA was analyzed by qPCR as described in the Gene expression analysis section. The amount of transcripts (%) bound to the antibody was calculated: 100 X 2^{-} [Ct(input) - Ct(IP)].

Luciferase promoter activity assay

Cells plated on a 6-well plate were co-transfected with 1 μg of renillia construct containing the promoter of interested gene and 0.2 μg of control cypridina construct using FuGENE HD transfection reagent (Promega). For co-transfection of luciferase constructs with siRNA, SE. Cell Line 4D-Nucleofector X Kit and 4D-Nucleofector system (Lonza) were used. 48 hr after transfection, the activity of luciferase was measured by LightSwitch dual assay system (SwitchGear Genomics) according to the manufacturer's protocol. Renilla luciferase activity was normalized by cypridina luciferase activity.

Expression constructs and mutagenesis

For expression studies, the coding sequence of human *SRPK2* (NM_001278273.1) was cloned into pKH3 vector (BclI/BamHI and MfeI/EcoRI), and the HA-SRPK2 from pKH3-SRPK2 was subcloned into pLNCX vector (NotI and SalI). To generate GST-tagged

SRPK2 protein for *in vitro* kinase assays, 454-521 amino acids of SRPK2 was cloned into pGEX-2T vector (EcoRI). pLX304-SRSF1-V5 and pCMV-SPORT6-mouse Srpk2 were obtained from Harvard PlasmID. To generate pLenti-Blast-mouse Srpk2, pCMV-SPORT6-Srpk2 was recombinated with pDONR223 vector by BP reaction (Gateway BP clonase II enzyme mix, Invitrogen), and the resulting pDONR223-Srpk2 was recombinated with pLenti-Blast-DEST vector by LR reaction (Gateway LR clonase II enzyme mix, Invitrogen). SRPK2 mutants (S494A, S494D, S497A, S494A/S497A, and K110M for human SRPK2; S488A/S491A for mouse Srpk2) were generated using QuickChange site-directed mutagenesis kit (Strategene). The constitutively active S6K1 construct (pKH3-S6K1-F5A/T389E/R3A) was previously described (Schalm and Blenis, 2002).

siRNA and shRNA expression

Pooled siRNAs (30 nM) were transfected using Lipofectamine RNAiMAX reagent. For the rescue experiment in Figure 4G, 10nM of siRNA targeting 3′ UTR of *SRPK2* (SASI_Hs01_00057789) was used. pLKO.1 shRNA constructs were from the RNAi Consortium (TRC) at the Broad Institute: shGFP (TRCN0000072181), shSRPK2#6 (TRCN0000006274, targeting 3′ UTR), and shSRPK2#10 (TRCN0000006278, targeting CDS). Results from shSRPK2#6 are shown as representative data unless otherwise stated.

CRISPR/Cas9 knockout

Each guide RNA sequence targeting human *SRPK2* (GCATTATACGGAGACAGCCT, GGATCCGCGGAATGCAGATA, and GACGCGTCAGTACCGCTCCA) was cloned into lentiCRISPRv2 vector (Sanjana et al., 2014). LAM 621-101 cells were infected with viral supernatants generated from lentiCRISPRv2 and selected with puromycin (10 μg/mL). Single cell cloning was performed by serial dilution in 96-well plates, followed by immunoblot analysis of SRPK2 to confirm knockout efficiency of multiple selected clones. Immunoblot result of the *SRPK2* knockout cells generated from the guide RNA, GCATTATACGGAGACAGCCT, is shown.

Generation of stable cell lines

HEK293T cells were co-transfected with the viral plasmid of interest with packaging and envelope plasmids according to the viral vectors (pLKO.1, pLenti-Blast and lentiCRISPRv2, lentiviral; pLNCX, retroviral) using Lipofectamine 2000 reagent as previously described (Csibi et al., 2014). Virus-containing supernatants were collected at 48 hr after transfection. Target cells were infected with 0.45 μM-filtered viral supernatant in the presence of 8 μg/mL polybrene for 24 hr. pLKO.1 or lentiCRISPRv2-infected LAM 621-101 cells were selected with 10 μg/mL puromycin. pLKO.1-infected A549 cells were selected with 2 μg/mL puromycin. pLenti-Blast-infected LAM 621-101 cells were selected with 30 μg/mL blasticidin. LAM 621-101 cells stably expressing empty vector or *TSC2* were provided by Elisabeth Henske (Siroky et al., 2012).

Cell lysis, fractionation, immunoprecipitation, and immunoblotting

Cells were washed twice with ice-cold PBS and homogenized on ice either in a regular lysis buffer (40 mM HEPES [pH 7.4], 1 mM EDTA, 120 mM NaCl, 0.5 mM DTT, 10 mM β-glycerophosphate, 1 mM NaF, 1 mM Na_3VO_4, 0.1% Brij-35, 0.1% deoxycholate, and 0.5% NP-40) or in a Triton X-100 lysis buffer (40 mM HEPES [pH 7.4], 1 mM EDTA, 120 mM NaCl, 0.5 mM DTT, 10 mM β-glycerophosphate, 1 mM NaF, 1 mM Na_3VO_4, and 1% Triton X-100) supplemented with protease inhibitors (250 μM PMSF, 5 μg/ml pepstatin A, 10 μg/ml leupeptin, and 5 μg/ml aprotinin). Cell lysates were cleared by centrifugation at 13,000 rpm at 4°C for 20 min. Isolation of nuclear versus cytoplasmic fractions was performed using an NE-PER kit (Thermo Fisher Scientific) according to the manufacturer's protocol. Protein concentration was measured by Bradford assay (Bio-rad) and the proteins were denatured by boiling for 10 min in a sample buffer. 15-30 μg of proteins were analyzed by immunoblotting as previously described (Csibi et al., 2014). Immunoblot signals were detected by Odyssey imaging system (LI-COR Biosciences) or enhanced chemiluminescence (ECL), and quantified by densitometry analysis of protein bands using Adobe Photoshop or Odyssey imaging system. Immunoblot images are representative of at least two independent experiments. Numbers below the immunoblot bands indicate the average band intensity of two representative immunoblot images normalized to the loading control.

For calf intestinal alkaline phosphatase (CIAP, New England Biolabs) treatment, cells were lysed in a CIAP buffer (New England Biolabs) supplemented with 1% Triton X-100, 1 mM DTT, and protease inhibitors. 50 μg of cell lysates were treated with 50 unit of CIAP at 37°C for 1 hr.

For immunoprecipitation of HA-S6K1, cells were lysed using a Triton X-100 lysis buffer (without DTT). 1 mg of cell lysates were incubated with primary antibodies at 4°C for 4 hr, followed by incubation with 50% slurry of protein A/G Sepharose beads (GE Healthcare Life Sciences) presaturated with lysis buffer for additional 1 hr. After rinsing three times with the lysis buffer, the immunoprecipitated proteins were used for further analysis.

Protein purification and *in vitro* kinase assays

For GST-SRPK2 protein purification, *E. coli* BL21 (New England Biolabs) was transformed with pGEX-2T-SRPK2 plasmids. The bacteria were grown at 28°C in 2x YTA medium containing 100 μg/ml ampicillin until A_{600} of 0.6-0.8, followed by 100 nM IPTG treatment for 2 hr to induce protein expression. The cells were harvested by centrifugation at 6,000 g at 4°C for 15 min and re-suspended in ice-cold PBS. The cells were lysed with sonicator, followed by incubation with 1% Triton X-100 at 4°C for 30 min. Cell lysates were

cleared by centrifugation at 12,000 g at 4°C for 10 min and incubated with 50% slurry of Glutathione Sepharose 4B (GE Healthcare Life Sciences) at 4°C for 2 hr. After rinsing three times with PBS, proteins were eluted with 1 mL elution buffer (50 mM Tris-HCl and 10 mM reduced glutathione, pH 8.0).

For S6K1 *in vitro* kinase assay, immunoprecipitated HA-S6K1 from HEK293E was incubated with 1 μg of GST-SRPK2 in a kinase assay buffer (25 mM Tris-HCl, [pH 7.4], 10 mM $MgCl_2$, 5 mM β-glycerophosphate, 2 mM DTT, and 100 μM ATP) containing 5 μCi [γ-^{32}P]-ATP (Perkin Elmer) at 30°C for 20 min. For CK1 *in vitro* kinase assay, 200 ng of GST-CK1 (EMD Millipore) was incubated with GST-SRPK2 in the kinase assay buffer containing 5 μCi [γ-^{32}P]-ATP at 30°C for 30 min. Samples were separated by SDS-PAGE, blotted onto nitrocellulose membrane, and subjected to autoradiography.

Immunofluorescence staining

Cells grown on a fibronectin and gelatin-coated glass coverslip in a 12-well plate were fixed with 4% methanol-free formaldehyde in PBS for 30 min. The cells were rinsed with PBS and permeabilized with 0.1% Triton X-100 in PBS for 10 min. Then the cells were blocked for 1 hr with the blocking buffer (50:50 mixture of 0.1% Triton X-100 buffer and LI-COR blocking buffer, LI-COR Biosciences) and incubated with anti-SRPK2 (1:100 dilution, BD Biosciences) and anti-pS6(S235/S236) (1:200 dilution, Cell Signaling Technology) antibodies in the blocking buffer overnight at 4°C. After rinsing three times with the Triton X-100 buffer, cells were incubated with the secondary antibodies conjugated with Alexa488 or with Alexa568 (1:1,000 dilution in the blocking buffer) at room temperature for 1 hr and washed three times with the Triton X-100 buffer. The cells were then incubated with 0.5 ug/mL Hoechst 33258 (Thermo Fisher) in PBS for 10 min, rinsed twice with PBS, and mounted onto the glass slides with a Dako mounting medium (Sigma-Aldrich). Images were taken using Nikon upright microscope or Zeiss laser scanning confocal microscope, and analyzed using MetaMorph software at Nikon Imaging Center (Harvard Medical School). For the quantification of cell numbers regarding nuclear-cytoplasmic localization of SRPK2, the average intensity of nuclear-SRPK2 (nucleus area is determined as overlapping with DAPI signal) was measured in control cells, and the cells containing nuclear-SRPK2 intensity above the average intensity of control were counted as nucleus.

Bioinformatics and *in silico* analysis

For the gene ontology (GO) enrichment analysis (Figure S2C and Table S2D), the list of genes was uploaded to the DAVID database website (https://david.ncifcrf.gov/) for biological pathway analysis. The criteria selected for the analysis were: gene identifier (OFFICIAL_GENE_SYMBOL), background genes (whole human genome), and analytic tool (functional annotation).

For the transcription factor enrichment analysis (Figure S2D), the list of genes was uploaded to the web-based gene set analysis toolkit (http://www.webgestalt.org/option.php) for identification of transcription factor binding site enrichments in upstream promoter regions. The criteria selected for the analysis were: organism (hsapiens), method (overrepresentation enrichment analysis, ORA), functional database (network, Transcription_factor_target), gene ID type (genesymbol), and reference set for enrichment analysis (affy_hta_2_0).

To analyze putative SRSF1, SRSF2, and SRSF3 binding sites (Table S1), the mRNA sequence of the transcripts was uploaded to the web server for mapping binding sites of RNA-binding proteins (http://rbpmap.technion.ac.il) (Paz et al., 2014). The criteria selected for the analysis were: RNA binding protein (Human/mouse motifs; SRSF1, SRSF2, and SRSF3) and Stringency level (high stringency).

QUANTIFICATION AND STATISTICAL ANALYSIS

Data obtained from the qPCR, immunoblot, immunofluorescence staining, crystal violet staining, HPLC, and proteomics were statistically analyzed using Student's t test and the graphs show mean ± SD. Data obtained from the whole transcriptome array and tumor xenograft assays were statistically analyzed using ANOVA analysis and the graphs show mean ± SEM. Detailed methods and p value for the statistical significance are described in the figure legends and methods details.

DATA AND SOFTWARE AVAILABILITY

The whole transcriptome microarray data have been deposited in NCBI's Gene Expression Omnibus and are accessible through GEO Series accession number GEO: GSE104335 (https://www.ncbi.nlm.nih.gov/geo/query/acc.cgi?acc=GSE104335).

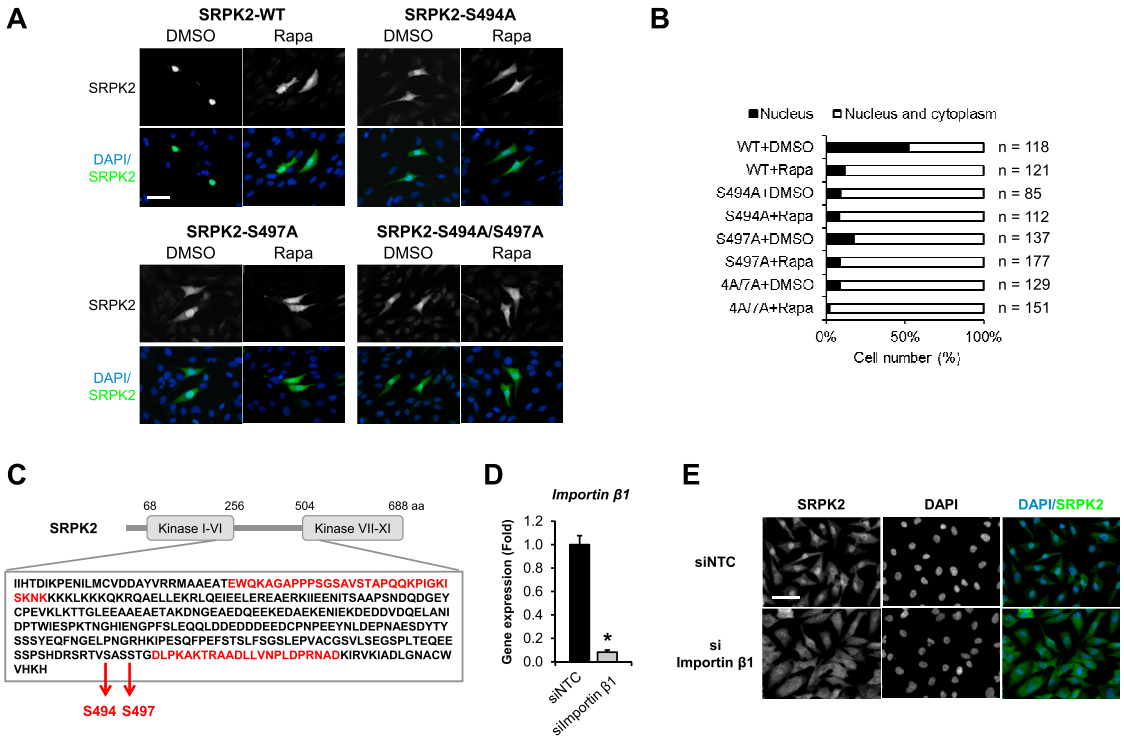

Figure S1. Further Characterization of SRPK2 Nuclear Localization, Related to Figure 3

(A) Immunostaining of SRPK2 (white) in LAM 621-101 cells expressing SRPK2-WT, S494A, S497A, or S494A/S497A. Endogenous *SRPK2* was knocked down with shSRPK2 targeting 3′ UTR. Cells were treated with vehicle or rapamycin (20 nM) for 2 hr. Bottom panels show the merged images of SRPK2 (green) with DAPI (blue). Scale bar, 50 μm.

(B) Quantification of nuclear-cytoplasmic distribution of SRPK2. The number of cells counted is indicated. Numbers for SRPK2-WT and S494A are also used in Figure 3G.

(C) Amino acid sequence of the SRPK2 linker region containing putative Importin α/β-dependent nuclear localization sequences (highlighted in red). Sequence was analyzed from http://nls-mapper.iab.keio.ac.jp/.

(D) Quantitative real-time PCR (qPCR) analysis of LAM 621-101 cells transfected with siRNAs targeting *Importin β1* or control. n = 3. *$p < 0.05$.

(E) Immunostaining of SRPK2 (white, left; green, right) in LAM 621-101 cells transfected with siRNAs targeting *Importin β1* or control. DAPI (white, middle; blue, right), nucleus. Scale bar, 50 μm.

A

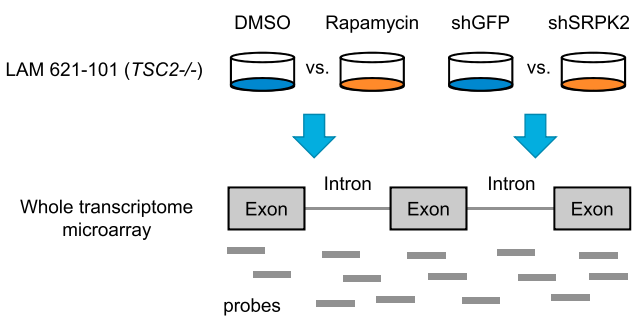

D

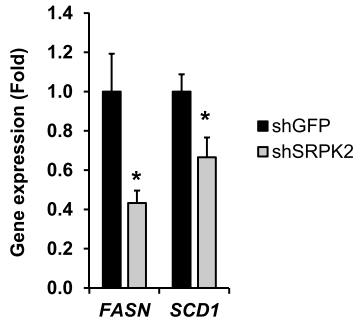

B

GO term	P value	Genes
GO:0060337~type I interferon signaling pathway	3.76E-17	*EGR1, IFITM1, IFITM2, OAS3, OAS1, OAS2, STAT1, PSMB8, IFI35, IFIT3, IFIT2, OASL, IFIT1, XAF1, MX1, IFI6*
GO:0009615~response to virus	1.04E-14	*IFIH1, IFITM1, IFITM2, OAS3, OAS1, IFI44, OAS2, CXCL12, DDX58, IFIT3, IFIT2, OASL, IFIT1, DDX60, EIF2AK2, MX1, FOSL1*
GO:0051607~defense response to virus	7.53E-11	*IFITM1, IFITM2, OAS3, PML, IFI44L, OAS1, OAS2, STAT1, IFIT3, IFIT2, PLSCR1, OASL, IFIT1, DDX60, EIF2AK2, MX1*
GO:0045071~negative regulation of viral genome replication	1.37E-10	*SRPK2, PLSCR1, IFIT1, OASL, IFITM1, IFITM2, OAS3, OAS1, EIF2AK2, MX1*
GO:0001666~response to hypoxia	1.00E-06	*EGR1, UCP2, PTK2B, PML, CAMK2D, ITGA2, THBS1, CXCL12, DPP4, ADA, CITED2, SOD2*
GO:0035456~response to interferon-beta	1.06E-06	*PLSCR1, IFITM1, IFITM2, XAF1, STAT1*
GO:0009612~response to mechanical stimulus	1.66E-06	*PTK2B, COL3A1, BDKRB1, THBS1, STAT1, CXCL12, FOSL1, CITED2*
GO:0045121~membrane raft	3.19E-06	*STAT6, ICAM1, PLSCR1, TNFRSF1A, PTK2B, SULF1, CLIP3, SDC4, BIRC3, DPP4, FAIM2, THY1*
GO:0060333~interferon-gamma-mediated signaling pathway	5.87E-06	*ICAM1, OASL, OAS3, PML, CAMK2D, OAS1, OAS2, STAT1*
GO:0031012~extracellular matrix	1.89E-05	*EFEMP1, COL3A1, ABI3BP, JUP, PLSCR1, APOE, F3, COL1A2, ADAMTS12, HSPA5, THBS1, MFAP4, LOXL1*
GO:0042493~response to drug	4.50E-05	*ICAM1, ASS1, HMGCS1, ITGA2, STAT1, ADA, SOD2, CCND1, PTK2B, FABP3, SRR, THBS1, FOSL1*
GO:0001889~liver development	8.48E-05	*ASS1, HMGCS1, ARF6, SEC63, ADA, CITED2, SOD2*
GO:0005615~extracellular space	9.44E-05	*CPM, ENPP2, C3, IL6ST, CSF1, COL3A1, OAS3, CXCL12, ABI3BP, ADA, TNFRSF1A, PAPPA, APOE, CTGF, THBS1, PTX3, LOXL1, ICAM1, SECTM1, EFEMP1, SERPING1, TNFRSF9, DKK1, F3, SULF1, COL1A2, C1RL, FABP3*
GO:0006955~immune response	2.56E-04	*SECTM1, IL1R1, C3, IFITM2, ENPP2, OAS3, OAS1, OAS2, IL7R, CXCL12, TNFRSF9, TNFRSF1A, THBS1, IFI6*
GO:0045087~innate immune response	3.14E-04	*SRPK2, IFIH1, CSF1, TRIM14, PML, SERPING1, C1S, DDX58, PTK2B, DDX60, C1RL, PTX3, MX1, EIF2AK2*
GO:0043066~negative regulation of apoptotic process	5.36E-04	*RARG, IL6ST, BIRC3, PLAC8, SOD2, CITED2, IFIT3, PLK2, UCP2, PTK2B, HSPA5, EIF2AK2, THBS1, FAIM2*
GO:0070542~response to fatty acid	5.62E-04	*ASS1, UCP2, CTGF, FABP3*
GO:0008284~positive regulation of cell proliferation	6.70E-04	*SRPK2, AKR1C2, RARG, RAC2, MVD, CTGF, PTK2B, IL6ST, CSF1, MLXIPL, THBS1, FOSL1, DPP4, PLAC8*
GO:0016020~membrane	7.37E-04	*BID, DYNC1LI2, IL1R1, IFITM1, IL6ST, CSF1, ARF6, OAS2, IL7R, SEC63, ADA, SLCO2A1, RAC2, MTCH2, APOE, CAMK2D, HSPA5, NT5E, DPP4, SLC30A6, GEMIN5, ICAM1, SVEP1, ACLY, TACC1, ATP6V1F, PLSCR1, CCND1, OASL, PARP9, PARP14, HSD11B1, SYTL4, EIF2AK2, DYNLRB1, EMP1*
GO:0009897~external side of plasma membrane	7.90E-04	*ICAM1, TNFRSF9, IL6ST, ITGA2, THBS1, IL7R, CXCL12, ADA, THY1*
GO:0045429~positive regulation of nitric oxide biosynthetic process	8.04E-04	*ICAM1, ASS1, PTK2B, PTX3, SOD2*

C

Transcription factor	P value	Genes
ISRE (Interferon-stimulated response element)	3.69E-07	*IFI44, DTX3L, DDX58, KCNIP3, IFIT2, IFIT3, PML, XAF1, DDX60, IFIH1, STAT6, THBS1, EPSTI1, AMMECR1*
IRF (Interferon regulatory transcription factor)	1.04E-05	*IFI44, DTX3L, F3, KCNIP3, IFI35, IFIT2, DDX60, PSMB8, RARG, CCND1, STAT6, THBS1*
IRF2 (Interferon regulatory transcription factor 2)	3.25E-05	*CITED2, IFI44, DTX3L, DDX58, IFIT2, IFIT3, XAF1, PSMB8, CCND1, EPSTI1*
ICSBP (Interferon consensus sequence-binding protein)	3.28E-04	*IFI44, DTX3L, EMP1, IFI35, IFIT3, ENPP2, PSMB8, IFIH1, STAT6, THBS1*
IRF7 (Interferon regulatory transcription factor 7)	1.38E-03	*DTX3L, DDX58, IFIT2, ARF6, XAF1, DDX60, OASL, STX11, EPSTI1*
P300	5.29E-03	*EMP1, HMGCS1, ARF6, PML, RARG, SRPK2, TNFRSF1A, CAMK2D*
c-REL	6.24E-03	*SEC63, CTGF, BIRC3, ICAM1, TNFRSF9, SDC4, STAT6, TACC1*
LMO2 (LIM domain only 2)	6.99E-03	*CITED2, NRK, PAQR5, RARG, SRM, VDR, FOSL1, B4GALT6*
FREAC2 (forkhead related activator 2)	8.50E-03	*CITED2, CTGF, EIF4EBP2, EMP1, EFEMP1, SULF1, ABI3BP, HSD11B1, IL6ST, JUP, VGLL3, PAPPA, ENPP2, RARG, CCND1, IFIH1, SRPK2, STAT6*
LEF1 (Lymphoid enhancer binding factor 1)	9.11E-03	*NEK7, EIF4EBP2, DKK1, HSD11B1, KBTBD4, UCP2, DGAT2*

(legend on next page)

Figure S2. Further Analysis of Whole-Transcriptome Microarray Results, Related to Figure 4

(A) Schematics of whole transcriptome microarray analysis on LAM 621-101 cells. One analysis was conducted on the conditions where cells were treated with rapamycin (20 nM) or vehicle for 24 hr. The second analysis was conducted on the conditions where cells stably express shRNAs targeting *SRPK2* or *GFP*. shGFP-expressing cells treated with vehicle were used in both analyses.

(B and C) Gene ontology (GO) (B) and transcription factor (C) analyses of the genes decreased by *SRPK2* knockdown from microarray analysis in (A).

(D) qPCR analysis of LAM 621-101 cells stably expressing shRNAs targeting *SRPK2* or *GFP*. n = 3. *p < 0.05.

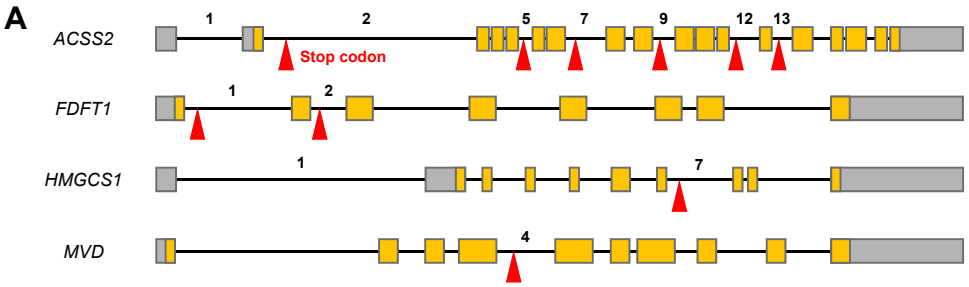

B

Gene	Intron	Probe ID	DMSO vs. Rapa		shGFP vs. shSRPK2	
			Splicing Index	P value	Splicing Index	P value
ACSS2	1	PSR20003138.hg.1	5.77	0.000038	2.29	0.000772
		PSR20003148.hg.1	2.57	0.019898	1.86	0.00671
		PSR20003149.hg.1	4.95	0.000472	1.69	0.012093
	2	PSR20003158.hg.1	5.46	0.000864	1.81	0.018888
		PSR20003160.hg.1	5.92	0.000065	2.1	0.000534
	5	PSR20003177.hg.1	7	0.003315	2.64	0.028254
	7	PSR20003183.hg.1	4.74	0.002181	2.03	0.023936
	9	PSR20003194.hg.1	3.57	0.000014	1.58	0.142718
	12	PSR20003199.hg.1	3.7	0.0047	2.15	0.028862
	13	PSR20003201.hg.1	2.07	0.000218	1.77	0.026223
		PSR20003202.hg.1	3.35	0.00057	2	0.001455
FDFT1	1	PSR08000911.hg.1	2.98	0.001191	2.44	0.002944
		PSR08000915.hg.1	3.02	0.002239	2.6	0.003673
		PSR08000916.hg.1	5.55	0.000354	3.63	0.003133
	2	PSR08000918.hg.1	2.23	0.004326	1.85	0.01738
HMGCS1	1	PSR05018576.hg.1	10.44	0.000079	1.77	0.003073
	7	PSR05018559.hg.1	7.49	0.000028	1.64	0.015075
MVD	4	PSR16018490.hg.1	5.1	0.000711	1.9	0.17202

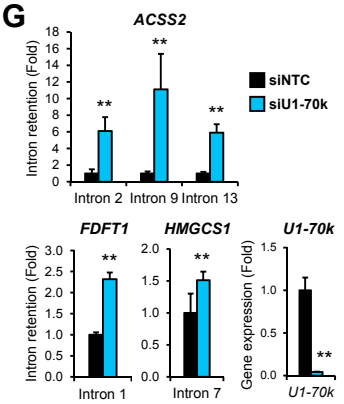

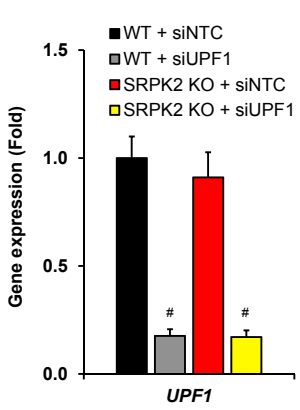

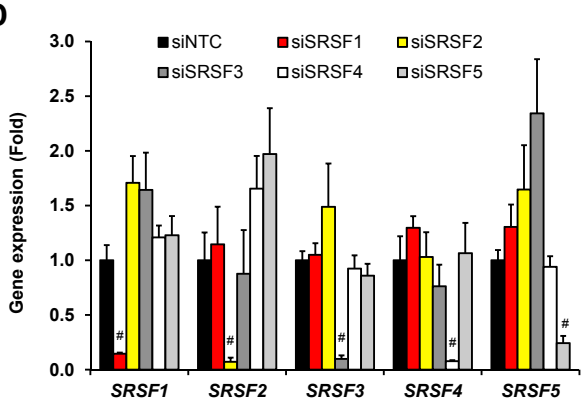

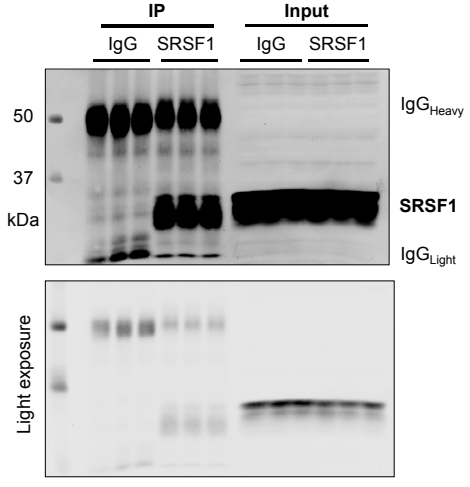

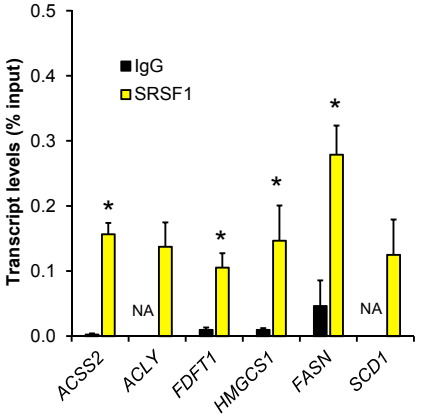

(legend on next page)

Figure S3. Further Characterization of Regulation of Lipogenic Gene Transcripts by mTORC1 and SRPK2, Related to Figures 4 and 5

(A) Schematics for the transcripts of *ACSS2* (NM_001242393), *FDFT1* (NM_004462), *HMGCS1* (NM_002130), and *MVD* (NM_002461). Introns marked with numbers represent the retained introns under rapamycin-treated and *SRPK2*-knocked down conditions from the whole transcriptome microarray analysis in Figure S2. Boxes and lines represent exons and introns, respectively. Grey and orange boxes represent untranslated region (UTR) and protein coding region (CDS), respectively. The first stop codons in each intron are indicated with red arrows.

(B) Probe ID and splicing index (SI) for the included introns in (A). SI = [Condition 1 (Probe intensity/Gene intensity)] / [Condition 2 (Probe intensity/Gene intensity].

(C and D) qPCR analysis of LAM 621-101 cells transfected with siRNAs targeting *UPF1*, each *SRSF*, or control.

(E and F) RNA-protein immunoprecipitation (RNA-IP) analysis of LAM 621-101 cells. Immunoprecipitation was performed with mouse IgG or anti-SRSF1 antibody. (E) Immunoblot analysis with anti-SRSF1 antibody (molecular weight of SRSF1 is ~35 kDa). Heavy and light chains of IgG are detected by mouse secondary antibody. 10% total cell lysate was loaded as an input. (F) qPCR analysis of RNA-IP products. NA, not applicable (expression not detected).

(G) qPCR analysis of LAM 621-101 cells transfected with siRNAs targeting *U1-70k* or control. Intron retentions identified in rapamycin-treated and *SRPK2*-knockdown samples in (A) were examined. Intron retention = (Expression of intron-included region) / (Expression of intron-excluded region).

n = 3. *$p < 0.05$, **$p < 0.01$, and #$p < 7E-06$.

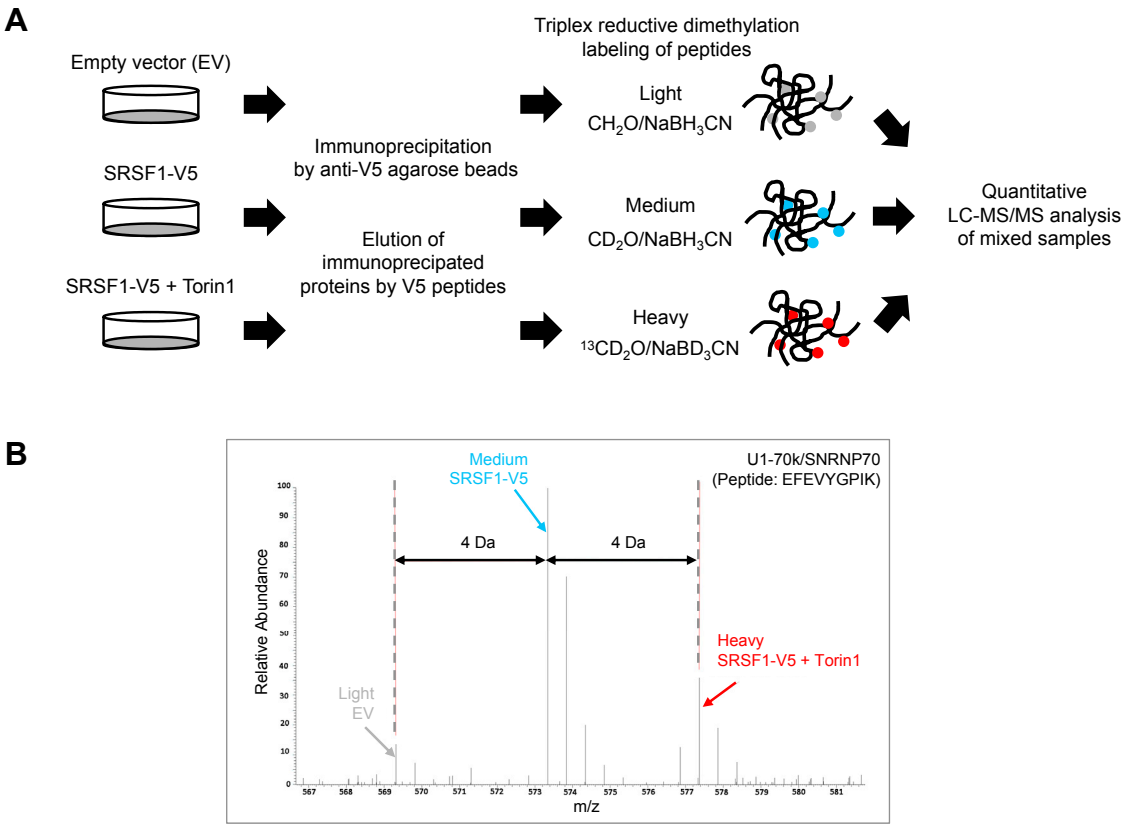

Figure S4. Interactome Analysis of SRSF1, Related to Figure 5

(A) Schematics of interactome analysis. HEK293E cells were transfected with empty vector or SRSF1-V5, followed by treatment with vehicle or Torin1 (250 nM) for 4 hr. SRSF1-binding proteins were co-immunoprecipitated by anti-V5 agarose beads and eluted by V5 peptides. Eluted proteins were digested with LysC and trypsin, isotopically labeled using triplex reductive dimethylation, mixed, and analyzed by mass spectrometry.

(B) MS spectra of EFEVYGPIK peptide from U1-70k/SNRNP70, which was identified to interact with SRSF1 and the interaction was decreased by Torin1.

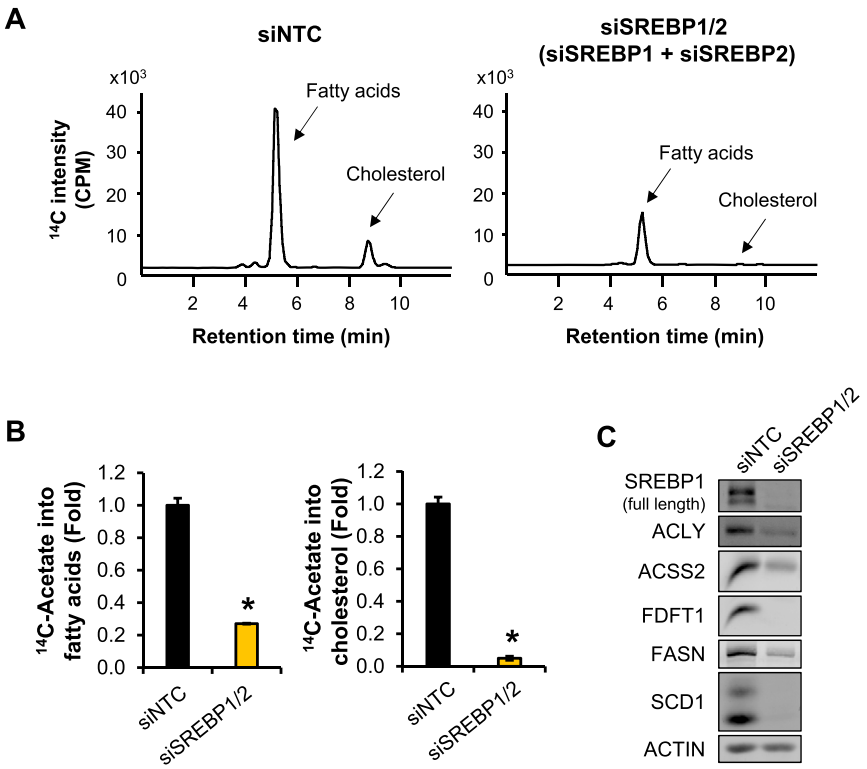

Figure S5. Further Characterization of Regulation of *De Novo* Lipogenesis by SREBP, Related to Figure 6

(A–C) LAM 621-101 cells were transfected with siRNAs targeting *SREBP1* and *SREBP2* (*siSREBP1/2*) or control. (A) HPLC analysis of radio-labeled fatty acids and cholesterol. (B) Quantification of the integrated peak areas in (A) normalized to internal control 13(S)-HODE. n = 2. *p < 0.05. (C) Immunoblot analysis with the indicated antibodies.

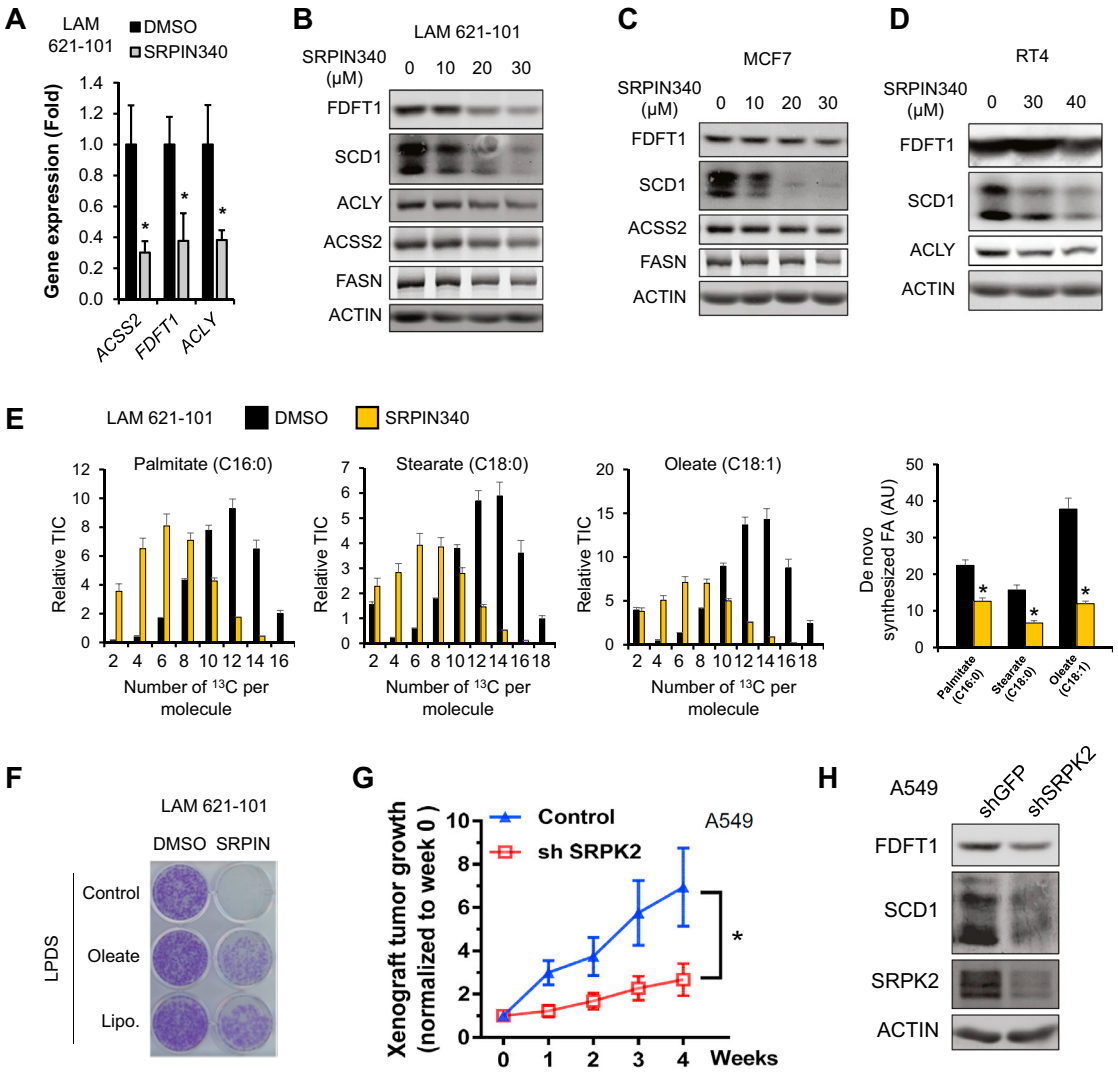

Figure S6. Further Characterization of SRPIN340, Related to Figure 7

(A) qPCR analysis of LAM 621-101 cells treated with SRPIN340 (30 μM) for 24 hr with serum starvation. n = 3.

(B–D) Immunoblot analysis of various cancer cell lines treated with the indicated concentration of SRPIN340 for 24 hr with serum starvation.

(E) LC-MS analysis of *de novo* fatty acid synthesis from U-^{13}C-glucose. LAM 621-101 cells were treated with vehicle (DMSO) or SRPIN340 (30 μM) for 48 hr with serum starvation. Left, Graphs represent relative total ion counts (TIC) of each fatty acid with the indicated number of ^{13}C-labeled carbons. Unlabeled fatty acids are not shown. Right, Graph represent *de novo* synthesized fatty acids (FA). Arbitrary unit (AU). n = 3.

(F) Crystal violet staining of LAM 621-101 cells treated with SRPIN340 (30 μM). Fatty acid-free albumin (25 μM; control), oleate-albumin (50 μM; oleate), or lipoprotein (25 μg/ml; Lipo.) was supplemented to the media. LPDS, Lipoprotein deficient serum.

(G) Xenograft tumor growth assays of A549 (KRAS-G12S lung cancer) cells stably expressing shRNAs targeting *SRPK2* or *GFP*. Graph represents the fold change of tumor size relative to week 0 (week 0 = tumor formation). n = 8 tumors.

(H) Immunoblot analysis of A549 cells stably expressing shRNAs targeting *SRPK2* or *GFP*.

*p < 0.05.

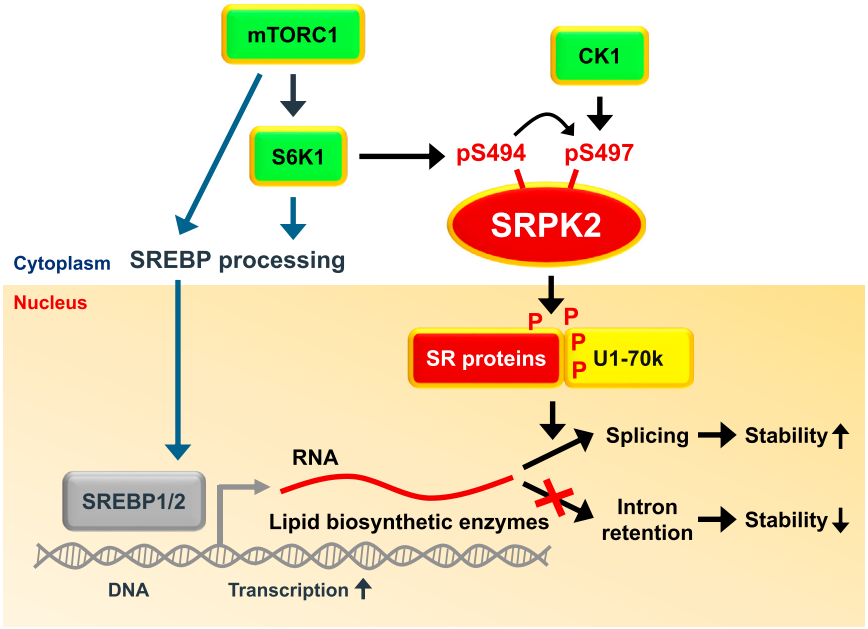

Figure S7. Proposed Model for the Regulation of Lipid Metabolism by mTORC1-SRPK2 Signaling Pathway, Related to Figure 7

mTORC1 signaling induces transcription of lipid biosynthetic enzymes through SREBP transcription factors. In addition, mTORC1 signaling phosphorylates and activates SRPK2. The activated SRPK2 promotes interaction of SR proteins with the spliceosomal protein U1-70k to induce efficient splicing of lipogenic pre-mRNAs. Inhibition of this signaling pathway leads to substantial intron retention of these genes, which in turn triggers NMD-mediated mRNA destabilization and thereby causes decreased protein expression.